

RESEARCH ARTICLE

Dorsal convergence of gastrula cells requires Vangl2 and an adhesion protein-dependent change in protrusive activity

Dianna J. Prince and Jason R. Jessen*

ABSTRACT

Lateral zebrafish hypoblast cells initiate dorsal convergence near mid-gastrulation and exhibit non-polarized morphologies, limited cell-cell contact and indirect migration trajectories. By late gastrulation, mesodermal cells become packed as they engage in planar cell polarity (PCP)-dependent movement. Here, we aimed to understand this transition in cell behavior by examining the relationship between protrusion dynamics and establishment of PCP and directed migration. We found that wild-type cells undergo a reduction in bleb protrusions near late gastrulation accompanied by a VANGL planar cell polarity protein 2 (Vangl2)-regulated increase in filopodia number and polarization. Manipulation of blebs is sufficient to interfere with PCP and directed migration. We show that Vangl2, fibronectin and cadherin 2 function to suppress blebbing. Vangl2 maintains ezrin b (Ezrb) protein levels and higher Ezrb activation rescues defective mediolateral cell alignment and migration paths in *vangl2* mutant embryos. Transplantation experiments show that loss of *vangl2* disrupts protrusion formation cell-autonomously while fibronectin acts non-autonomously. We propose that dorsal convergence requires the coordinated action of Vangl2, Ezrb and cell-adhesion proteins to inhibit blebs and promote polarized actin-rich protrusive activity and PCP.

KEY WORDS: Vangl2, Fibronectin, Ezrin b, Protrusion, Polarity, Migration

INTRODUCTION

Vertebrate gastrulation includes several conserved morphogenetic cell movements acting in concert to shape the embryonic body plan (Solnica-Krezel, 2005). For zebrafish (*Danio rerio*), convergence and extension are the major movements required to narrow and extend embryonic tissues along the mediolateral and anterior-posterior axes, respectively. Underlying convergence and extension are polarized cell behaviors necessary for directed cell migration and intercalation events (Jessen and Solnica-Krezel, 2005; Keller, 2002). Notably, the elongation and mediolateral alignment of ectodermal and mesodermal cell populations is a hallmark of efficient zebrafish gastrulation movements. These processes are regulated by complex interactions among a conserved group of planar cell polarity (PCP) proteins that includes VANGL planar cell polarity protein 2 (Vangl2) and components of a glypican 4-regulated non-canonical Wnt signaling pathway (Roszko et al., 2009). Although the general requirement for PCP proteins such as


Vangl2 during dorsal convergence is clear, many details are lacking. For example, while PCP signaling is thought to impact organization of the actin cytoskeleton, little is known regarding the membrane protrusions used by gastrula cells or how protrusive activity relates to PCP establishment and directed migration.

During zebrafish gastrulation, internalized hypoblast cells migrate toward the animal pole until shortly after 75% epiboly when their migration trajectories become dorsally biased (Sepich et al., 2005). At this stage, mesendodermal cells are not morphologically polarized and exhibit meandering or indirect dorsal migration paths (Jessen et al., 2002). The movement of these cells is also characterized by reduced cell-cell contact and cohesion compared with later gastrulation stages (Fig. 1A). Neither the onset of dorsal convergence nor these initial migration events depend on the function of the core PCP protein Vangl2 (Jessen et al., 2002; Sepich et al., 2005). At 80% epiboly (mid-gastrulation) there is minimal fibronectin extracellular matrix (ECM), and it is localized between the epiblast and hypoblast germ layers (Latimer and Jessen, 2010). Therefore, the deepest layer of mesendodermal cells is not in contact with a fibronectin adhesive substrate. At late gastrulation, deep lateral mesendodermal cells (now classified as mesodermal cells) move closer to the embryonic body axis and adopt a planar polarized morphology, as evidenced by higher length-width ratios (LWRs) and mediolateral cell body alignment (Jessen et al., 2002; Marlow et al., 2002; Topczewski et al., 2001). This change in morphology is accompanied by greater cell packing, a straightening of migration trajectories and the appearance of fibrillar fibronectin beneath the deep mesodermal cell layer (Jessen et al., 2002; Latimer and Jessen, 2010). Prior to these events, Vangl2 protein shifts from predominantly cytoplasmic expression to a widespread plasma membrane distribution (Roszko et al., 2015). Despite being packed, lateral gastrula cells exhibit extensive membrane-protrusive activity throughout gastrulation (Lin et al., 2010; Love et al., 2018). The mesodermal cells in PCP mutants such as *vangl2* (*trilobite*) fail to undergo the late gastrulation transition and instead remain rounder and less packed, and continue to meander as they move dorsally (Fig. 1A,B) (Jessen et al., 2002; Roszko et al., 2015; Sepich et al., 2000). Notably, gastrula-stage *vangl2* mutant embryos have a reduced fibronectin ECM compared with wild type (Dohn et al., 2013; Love et al., 2018; Williams et al., 2012).

Observations by J. P. Trinkaus and colleagues showed that migrating cells in the *Fundulus heteroclitus* gastrula embryo exhibit a preponderance of filopodia, lamellipodia and filolamellipodia membrane protrusions but fewer blebs (Trinkaus et al., 1992). We have reported that late gastrulation stage zebrafish ectodermal cells also generate primarily filopodia-like and large lamellipodia-like protrusions (Love et al., 2018). Proper ectodermal cell protrusion formation and polarization is Vangl2 dependent and requires the presence of a fibronectin ECM (Love et al., 2018). Data from early gastrulation stage mesendodermal cells (before 80% epiboly)

Department of Biology, Middle Tennessee State University, Murfreesboro, TN 37132, USA.

*Author for correspondence (jason.jessen@mtsu.edu)

 J.R.J., 0000-0002-8209-3620

Received 1 July 2019; Accepted 29 October 2019

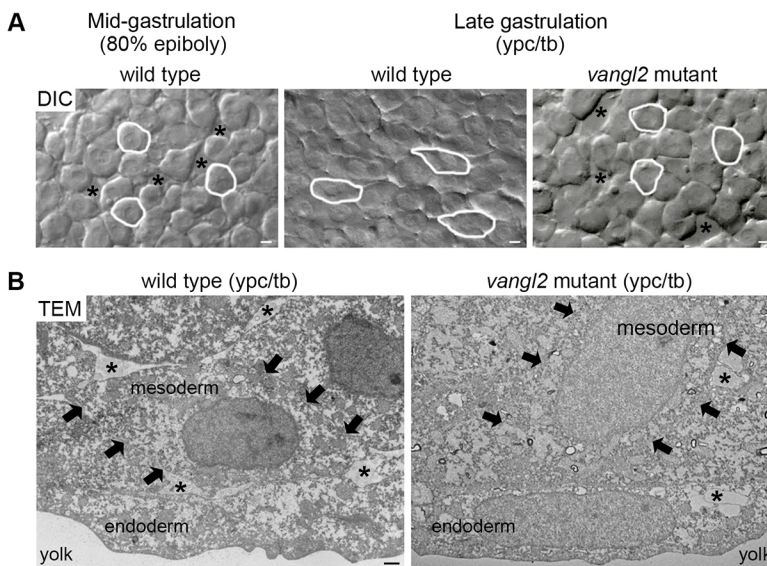


Fig. 1. Vangl2-dependent changes in mesodermal cell behavior at late gastrulation. (A) Single-frame DIC time-lapse images highlighting morphological differences between wild-type mesodermal cells at mid-gastrulation and mesodermal cells at late gastrulation (Jessen et al., 2002; Roszko et al., 2015). The mesoderm of a late gastrulation stage *vangl2^{vu67/vu67}* mutant embryo is shown for comparison. Images are oriented as shown in Fig. 2A with dorsal to the right and anterior to the top. Selected cells are outlined to show elongation and alignment relative to the dorsal-ventral body axis. Asterisks mark intercellular gaps. Scale bars: 5 μ m. (B) Normal and defective PCP, as viewed in cross-sectioned images (6500 \times magnification) of late gastrulation wild-type and *vangl2^{m209/m209}* mutant deep mesodermal cells taken using transmission electron microscopy (TEM). Black arrows indicate the boundaries of single mesodermal cells. Asterisks indicate the presence of ECM between cells. Scale bar: 1 μ m.

migrating toward the animal pole suggest that actin-rich protrusions are required for directed migration (runs) while blebs are associated with tumbling phases of cell movement (Diz-Muñoz et al., 2016). Here, the balance between blebbing and actin-rich protrusion formation is regulated by ezrin b (Ezrb). Furthermore, it has been proposed that blebs have an exploratory function and are used to promote cell reorientation along the path of migration. This is in contrast to zebrafish primordial germ cells that solely use blebs to achieve directional movement along a chemotactic gradient (Blaser et al., 2006). Blebs are unique from actin-rich protrusions because they form as a result of actomyosin contractility and hydrostatic pressure that cause plasma membrane separation from cortical actin (Fackler and Grosse, 2008). While bleb protrusions do not appear to require integrin-mediated adhesion to the ECM (Diz-Muñoz et al., 2010), their formation is influenced by the physical or mechanical cellular microenvironment. Current *in vitro* data suggest that at low matrix adhesion cells may predominantly form bleb protrusions, whereas, at high adhesion, cells often switch to actin-based protrusive activity (Tozluoğlu et al., 2013). Loss of integrin fibronectin receptors in the zebrafish paraxial mesoderm causes formation of a higher number of blebs (Dray et al., 2013). Cadherin function and subsequent mechanotensive effects on the actin cytoskeleton also regulate ECM structure and tissue rigidity (Dohn et al., 2013; Dzamba et al., 2009; Weber et al., 2011). In addition, a gradient of N-cadherin/cadherin 2 (Cdh2)-mediated cell adhesion may influence the dorsal migration of lateral mesoderm (von der Hardt et al., 2007).

In this study, we specifically examined the transition to PCP-dependent mesodermal cell migration to determine the types of membrane protrusions involved and their regulation by Vangl2 and cell adhesion proteins. Our data show that underlying this transition is a reduction in blebbing and a corresponding increase in polarized actin-rich filopodia. These protrusion changes required the function of Vangl2, fibronectin and Cdh2. Increasing the number of bleb protrusions by interfering with membrane-cortex attachment was sufficient to inhibit PCP and directed migration at late gastrulation stages. We also show that *vangl2* regulates blebbing cell-autonomously, likely through effects on Ezrb protein expression levels. Together, our findings demonstrate that proper membrane-protrusive activity is essential for PCP and for efficient dorsal convergence of the lateral mesoderm.

RESULTS

Vangl2-dependent polarization of filopodia at late gastrulation

Initiation of dorsal convergence by mesodermal cells occurs abruptly at around 75% epiboly (Sepich et al., 2005) (Movie 1). The *vangl2/trilobite* mutant PCP phenotype is not detected until near yolk-plug closure (ypc) and prior to the tailbud (tb) stage, marking the end of gastrulation (Sepich et al., 2000). Therefore, throughout this study we used the stages of 80% epiboly (mid-gastrulation) and ypc/tb (late gastrulation) to examine cell behaviors during the transition to PCP-dependent migration. We examined lateral cells located near the embryo equator and at $\sim 90^\circ$ (80% epiboly) or $40\text{--}60^\circ$ (ypc/tb) from the notochord (Fig. 2A). Paraxial pre-somitic mesodermal cells were excluded from our study because their behaviors are distinct from lateral cells engaged in directed migration (Williams and Solnica-Krezel, 2017; Williams et al., 2018). First, actin-rich protrusions were imaged using time-lapse confocal microscopy and mosaic expression of Lifeact-GFP to label actin (Fig. 2A) (Love et al., 2018; Riedl et al., 2008). Protrusive organelles were broadly classified as spike- or finger-like filopodia, or larger sheet-like lamellipodia/filolamellipodia (henceforth large protrusions). We found there was a Vangl2-independent increase in the number of filopodia per cell at the ypc/tb stage compared with 80% epiboly (Fig. 2B; Movies 2 and 3). By contrast, there was no difference in the number of large protrusions produced by wild-type cells at these stages (Fig. 2C). We next quantified membrane protrusion polarity in relation to the dorsal body axis, which for ypc/tb stage wild-type mesodermal cells, is also the path of migration. Protrusions were classified as polarized if they were oriented $\pm 45^\circ$ from a line drawn through the cell and perpendicular to the notochord (Fig. S1). The percentage of polarized dorsal, or leading edge, protrusions was similar between 80% epiboly and ypc/tb stage embryos (Fig. 2D,E). Large protrusion polarity in particular was highly variable from cell to cell (Fig. 2E). However, the number of mediolaterally biased (dorsal+ventral) filopodia was increased at late gastrulation (Fig. 2D), indicating that many were oriented ventrally. Filopodia polarization was significantly lower in *vangl2* mutant embryos. These data indicate that dorsal-biased protrusion polarity alone cannot account for the convergence of lateral mesodermal cells. In addition, our results suggest that

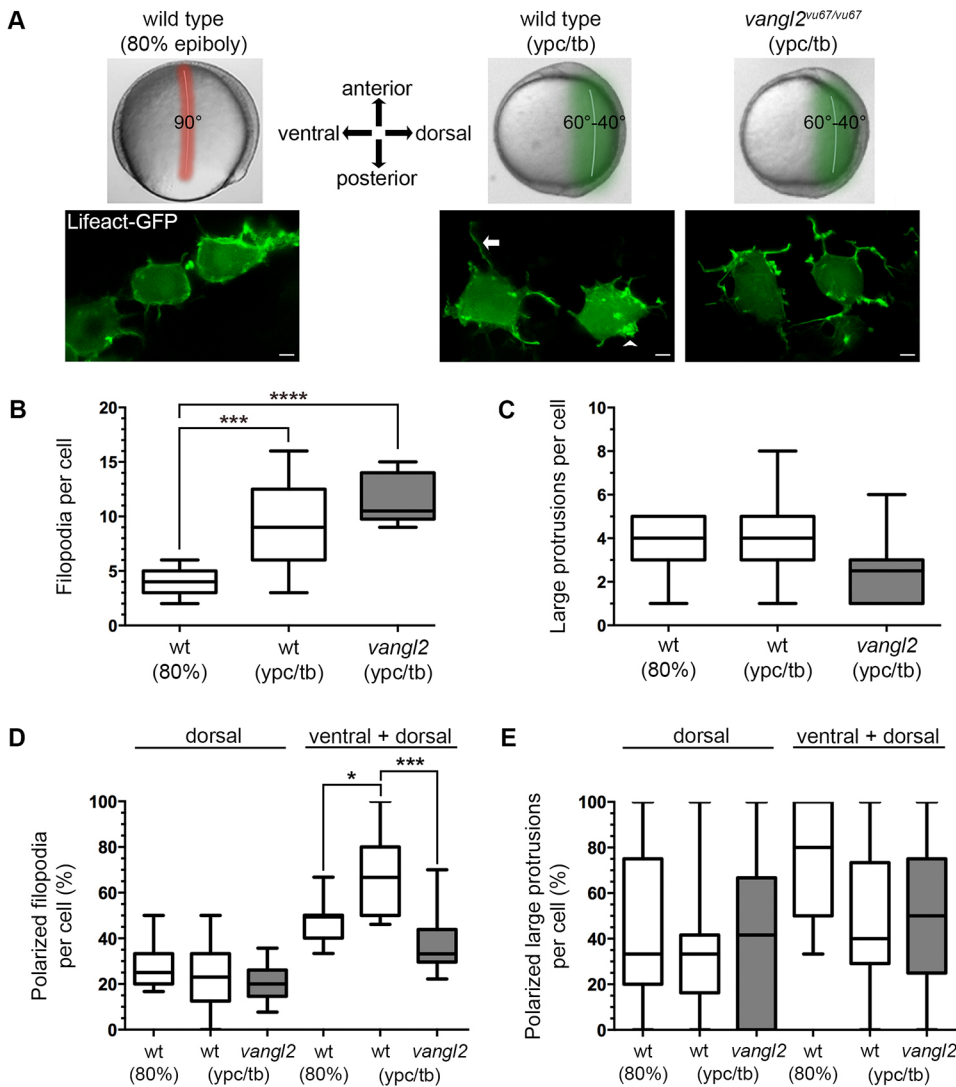


Fig. 2. Vangl2 is required for polarized filopodia at late gastrulation. (A) Live embryo images of gastrulation stages and embryonic regions analyzed in this study (top). Confocal live cell images of lateral mesendodermal and mesodermal cells at 80% epiboly and the ypc/tb stage, respectively (bottom). Filopodia (arrow) and larger actin-rich protrusions (arrowhead) are labeled with Lifect-GFP. The images are oriented in relation to the anterior-posterior and dorsal-ventral embryonic body axes. Scale bars: 5 μ m. (B,C) Quantitation of filopodia and large protrusion numbers in wild-type and *vangl2^{vu67/vu67}* mutant embryos (wild type at 80% epiboly, $n=7$ cells, 6 embryos; wild type at ypc/tb, $n=13$ cells, 10 embryos; *vangl2* mutant, $n=10$ cells, 6 embryos). (D,E) Percentage of polarized filopodia and large protrusions formed in relation to the dorsal-ventral body axis. Box plots show the interquartile dataset, the median and the data range. * $P<0.05$, *** $P<0.001$, **** $P<0.0001$; unpaired Student's t -test with Welch's correction.

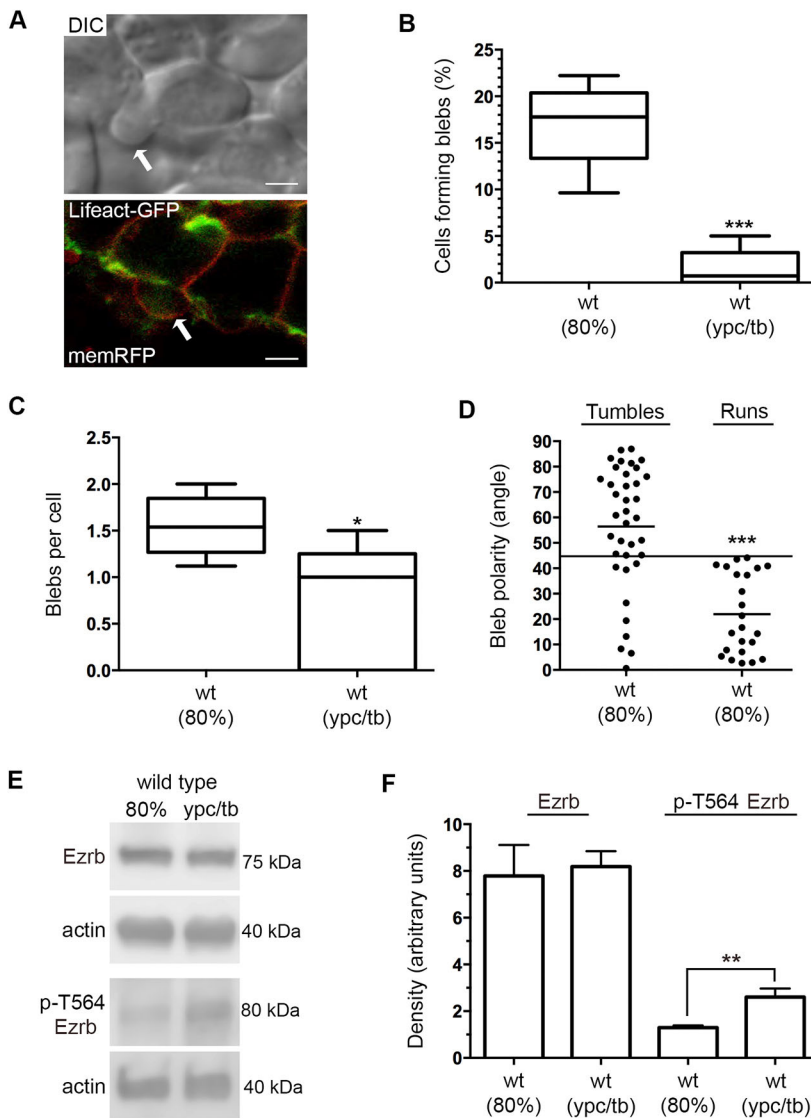
mediolaterally oriented filopodia may contribute to directed migration. As noted earlier, lateral mesodermal cells are not simply migrating dorsally, they are also engaged in packing behaviors as they align perpendicular to the embryonic body axis.

Differences in bleb protrusion formation by lateral gastrula cells

Our previous data showed that lateral ectodermal gastrula cells form few bleb-like membrane protrusions as they migrate dorsally (Love et al., 2018). Unlike the ectoderm, however, lateral mesendodermal cells exhibit less contact at mid-gastrulation and do not pack until later stages. Differential interference contrast (DIC) microscopy and time-lapse imaging were used to analyze the blebbing activity of wild-type mesendodermal and mesodermal cells. Our ability to identify protrusions as blebs was verified using confocal imaging of mesodermal cells that were mosaically labeled with Lifect-GFP and membrane-targeted RFP (memRFP) (Fig. 3A). Blebs are characterized by their hemispherical appearance and initial lack of actin (Fackler and Grosse, 2008). We found that the number of wild-type cells with bleb protrusions was higher at 80% epiboly compared with the ypc/tb stage (Fig. 3B; Movies 4 and 5). The number of blebs formed per cell was also higher at 80% epiboly

(Fig. 3C). We next quantified the polarity of all bleb protrusions at 80% epiboly. Protrusions were classified as polarized if they were oriented $\pm 45^\circ$ from a line drawn through the cell and parallel to the path of migration (Fig. S1). The number of polarized leading edge blebs was 26.8%, indicating a lack of polarity. Dissecting these data further, we analyzed blebbing and protrusion polarity as mesendodermal cells engaged in either tumbles or runs. We found that cells formed blebs during both phases of movement, but whereas only 24% of blebs were polarized when cells were tumbling, 100% of blebs were polarized during the run phase (Fig. 3D). These results indicate that dorsal convergence of mesendodermal cells involves both actin-rich protrusions and blebs.

We reasoned that loss of bleb protrusions at late gastrulation is associated with decreased ezrin protein expression or activation. Ezrin is a member of the ezrin-radixin-moesin family and functions to link the plasma membrane to cortical actin (Bretscher et al., 1997). Cytoskeletal association with the plasma membrane is promoted by phosphorylation of ezrin at T567 (Jayasundar et al., 2012). Zebrafish Ezrb is expressed throughout the ectoderm and mesoderm of gastrula stage embryos (Link et al., 2006), and Ezrb knockdown has been shown to promote mesendodermal cell bleb formation at the expense of actin-rich



protrusions (Diz-Muñoz et al., 2010). Total protein extracts were generated from 80% epiboly and *ypc/tb* stage wild-type embryos and analyzed for both Ezrb and phospho-Ezrb (T564 in zebrafish) using western blot. The data show that, although the total level of Ezrb protein is unchanged, there is a significant increase in phosphorylated Ezrb at the *ypc/tb* stage compared with 80% epiboly (Fig. 3E,F). These data support the notion that the reduction in bleb protrusive activity at late gastrulation may be due to increased Ezrb activation.

Manipulation of bleb protrusions influences PCP and dorsal convergence

The reduction in blebbing at late gastrulation suggests this type of protrusive activity is not required or may be inhibitory for PCP-dependent mesodermal cell migration. To test this further, wild-type embryos were injected with synthetic mRNA encoding a constitutively active form of Ezrb (*ca-ezrb*; T564D) to inhibit blebbing (Diz-Muñoz et al., 2016; Gautreau et al., 2000). Alternately, embryos were injected with an *ezrb* antisense morpholino (MO) oligonucleotide to interfere with Ezrb expression and increase bleb formation (Diz-Muñoz et al., 2010; Link et al., 2006). Polarized cell behaviors and directed migration were then analyzed in 80% epiboly

and *ypc/tb* stage embryos. As previously reported, Ezrb knockdown embryos exhibited a strong convergence and extension phenotype characterized by shortened and broadened body axes (Fig. 4A, Fig. S2) (Link et al., 2006). Furthermore, our data show that expression of activated Ezrb inhibits bleb formation at 80% epiboly, while Ezrb knockdown promotes blebbing at the *ypc/tb* stage (Fig. 4B, Figs S3 and S4; Movies 6 and 7). The number of blebs produced per cell was decreased by *ca-ezrb* but unaffected by *ezrb* MO (Fig. S6). Having confirmed that manipulation of Ezrb activity affects blebbing in lateral gastrula cells, we asked whether Ezrb function is required for PCP establishment. Ezrb knockdown disrupted PCP, as indicated by reduced cellular LWRs and mediolateral alignment (MLA) (Fig. 4A,C,D, Figs S1 and S7). We next performed cell tracking to compare how increasing or decreasing bleb protrusion formation affected cell migration trajectories. Directness values were determined by dividing the Euclidean migration distance by the total distance. At 80% epiboly, wild-type mesendodermal control cells moved dorsally along highly indirect trajectories, with some cells moving ventrally at times, while cells in *ca-ezrb* mRNA-injected embryos had increased directness (Fig. 4E,F). Conversely, our data show that when bleb formation was stimulated by Ezrb knockdown, *ypc/tb* stage mesodermal

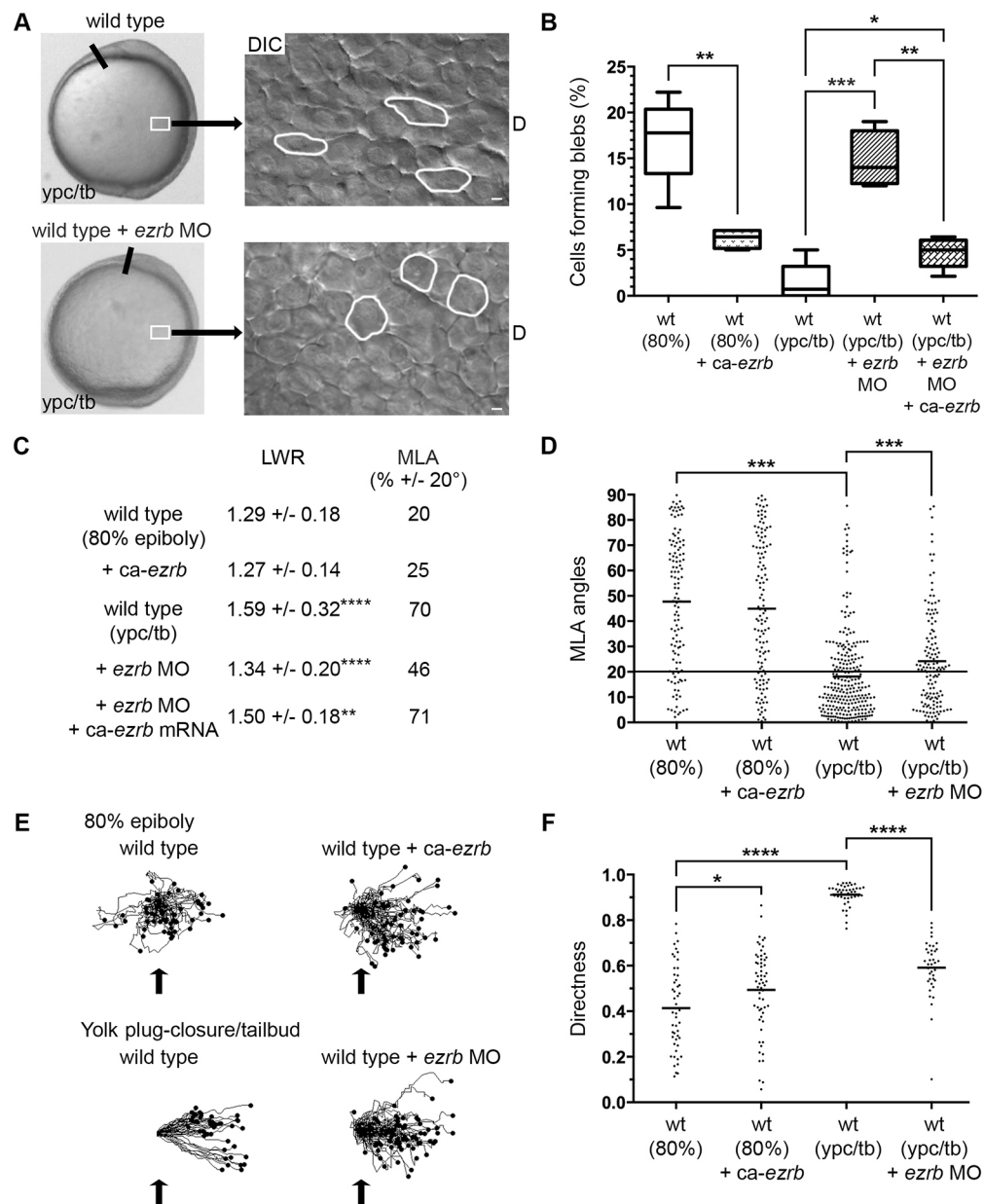


Fig. 4. Greater bleb protrusion formation disrupts PCP and directed migration. (A) Live embryo and DIC control images (reproduced from Fig. 2A and Fig. 1A, respectively) of lateral mesodermal cells at the *ypc/tb* stage. Control and wild-type embryo injected with *ezrb* MO. White boxes indicate approximate position of microscopic analysis. DIC images are oriented as shown in Fig. 2A with dorsal to the right and anterior to the top. Select cells are outlined to show elongation and alignment relative to the dorsal-ventral body axis. D, dorsal. Scale bars: 5 μ m. (B) Percentage of cells forming bleb protrusions during the 15 min time-lapse imaging (wild type at 80% epiboly+*ca-ezrb*, $n=560$ cells, 4 embryos; wild type at *ypc/tb*+*ezrb* MO, $n=400$ cells, 4 embryos; wild type at *ypc/tb*+*ezrb* MO+*ca-ezrb* mRNA, $n=140$ cells, 5 embryos). (C) PCP quantitation of lateral mesodermal and mesodermal cells (wild type at 80% epiboly, $n=150$ cells, 4 embryos; wild type at 80% epiboly+*ca-ezrb*, $n=126$ cells, 4 embryos; wild type at *ypc/tb*, $n=265$ cells, 8 embryos; wild type at *ypc/tb*+*ezrb* MO, $n=137$ cells, 4 embryos; wild type at *ypc/tb*+*ezrb* MO+*ca-ezrb* mRNA, $n=93$ cells, 4 embryos). (D) MLA data from C depicted as individual data points (in degrees). Long black line indicate 20°. (E) Cell migration tracks toward the dorsal body axis. Origins (black arrows) were standardized for comparison. (F) Directness values for individual cells (wild type at 80% epiboly, $n=50$ cells, 3 embryos; wild type+*ca-ezrb* at 80% epiboly, $n=60$ cells, 3 embryos; wild type at *ypc/tb*, $n=44$ cells, 3 embryos; wild type+*ezrb* MO at *ypc/tb*, $n=77$ cells, 3 embryos). Box plot (B) shows the interquartile dataset, the median and the data range. Scatter plots (D,F) show individual data points and average values. * $P<0.05$, ** $P<0.01$, *** $P<0.001$, **** $P<0.0001$; unpaired Student's *t*-test with Welch's correction, except D (Watson non-parametric two-sample U^2 test).

cells had decreased migration directness (Fig. 4E,F). These data show that the protrusive activity of blebs is inhibitory to PCP establishment and directed migration, and suggest that mechanisms exist to inhibit blebbing by late gastrulation stage mesodermal cells. Such mechanisms will likely affect *Ezrb* function.

Cell-adhesion proteins are required to suppress blebbing at late gastrulation

Directed migration and membrane-protrusive activity are influenced by both ECM geometry (density and cross-linking) and cell adhesiveness to matrix proteins (Charras and Sahai, 2014). The collective movement of cell populations also involves extensive

cell-cell interactions that must be coordinated with protrusive activity (Friedl and Gilmour, 2009; Mishra et al., 2019). In zebrafish, the quantity and fibrillar assembly of fibronectin increases at late gastrulation stages (Latimer and Jessen, 2010). Moreover, Cdh2 is strongly expressed in gastrula mesodermal cells (Harrington et al., 2007; Warga and Kane, 2007) and plasma membrane cadherin expression is significantly higher at *ypc/tb* compared with 80% epiboly (Fig. 5A,B). We hypothesized that PCP-dependent mesodermal cell migration requires both fibronectin and Cdh2. Antisense morpholinos (MOs) were used to address the function of these adhesion proteins. For fibronectin, a combination of MOs was used to knockdown the protein expression of both fibronectin genes (*fn1a* and *fn1b*) (Jülich et al., 2005; Latimer and Jessen, 2010; Love et al., 2018). For Cdh2, embryos were injected with an MO that binds the *cdh2* 5' UTR and effectively phenocopies germline mutant defects (Lele et al., 2002). We found that late gastrulation stage *fn1a/1b* and *cdh2* morphant mesodermal cells had reduced LWRs and MLA, indicative of disrupted PCP (Fig. 5C-E, Figs S1 and S7). In contrast to loss of fibronectin (Love et al., 2018), Cdh2 knockdown did not disrupt PCP in lateral ectodermal cells (wild type, LWR=1.63, MLA±20°=86%, n=151 cells, 3 embryos; wild

type+*cdh2* MO, LWR=1.58, MLA±20°=84%, n=141 cells, 3 embryos). Notably, injection of *fn1a* and *fn1b* synthetic mRNA did not affect cellular LWRs but promoted the MLA of 80% epiboly stage mesodermal cells (Fig. 5D,E). Given the effects of fibronectin and Cdh2 knockdown on mesodermal PCP, we reasoned there may be an inverse relationship between adhesive forces and formation of bleb protrusions at late gastrulation. Indeed, our data show that a higher percentage of *fn1a/1b* and *cdh2* morphant mesodermal cells formed blebs compared with wild type (Fig. 6A, Fig. S3; Movies 8 and 9). The bleb and PCP phenotypes were also observed in *cdh2^{tm101/tm101}* mutants (Fig. S8). Unlike fibronectin knockdown, *cdh2* MO-injected embryos had a greater number of blebs per mesodermal cell compared with wild type (Fig. S6). These results suggest that the ability of cells to adhere to each other or to the ECM functions to suppress blebbing. To examine this further, we asked whether fibronectin overexpression suppresses bleb protrusion formation at mid-gastrulation. The percentage of mesodermal cells with blebs at 80% epiboly was reduced in *fn1a/1b* mRNA-injected wild-type embryos compared with controls (Fig. 6B, Fig. S4; Movie 10). Analysis of time-lapse images showed that *fn1a/1b* and *cdh2* morphant mesodermal cells had decreased

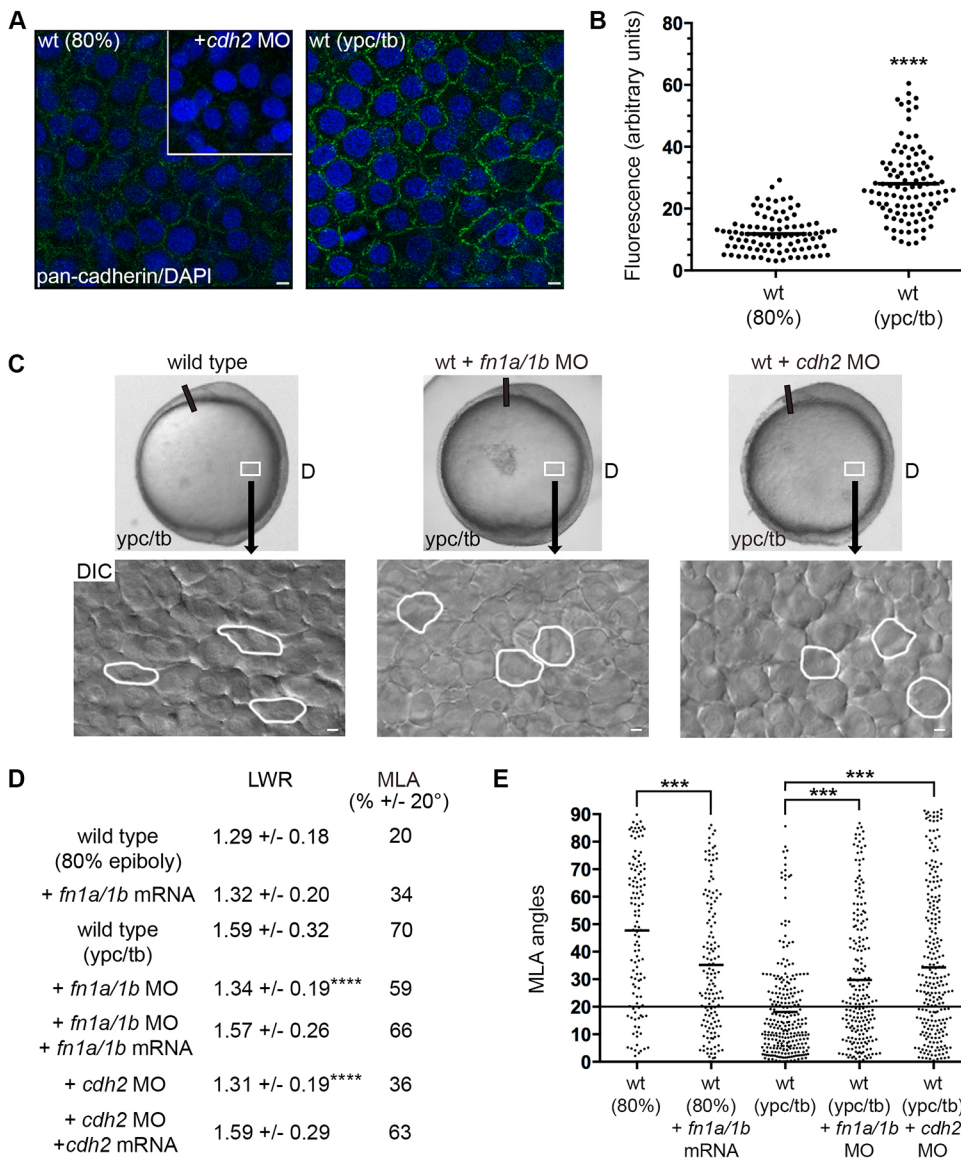


Fig. 5. Fibronectin and Cdh2 regulate mesodermal PCP. (A,B) Greater plasma membrane expression of Cdh2 in wild-type embryos at the *ypc/tb* stage compared with 80% epiboly. Inset shows antibody labeling in the *cdh2* morphant. (C) Live embryo and DIC control images (reproduced from Fig. 2A and Fig. 1A, respectively) of lateral mesodermal cells at the *ypc/tb* stage. Control and wild-type embryos injected with *fn1a/1b* MO and *cdh2* MO. White boxes indicate approximate position of microscopic analysis. DIC images are oriented as shown in Fig. 2A, with dorsal to the right and anterior to the top. Selected cells are outlined to show elongation and alignment relative to the dorsal-ventral body axis. D, dorsal. (D) PCP quantitation of lateral mesodermal and mesodermal cells (wild type at 80% epiboly+*fn1a/1b* mRNA, n=140 cells, 5 embryos; wild type at *ypc/tb*+*fn1a/1b* MO, n=211 cells, 5 embryos; wild type at *ypc/tb*+*fn1a/1b* MO+*fn1a/1b* mRNA, n=73 cells, 4 embryos; wild type at *ypc/tb*+*cdh2* MO, n=238 cells, 4 embryos; wild type at *ypc/tb*+*cdh2* MO+*cdh2* mRNA, n=60 cells, 3 embryos). (E) MLA data from D depicted as individual data points (in degrees). Long black line indicates 20°. Scatter plots (B,E) show individual data points and average values. ****P*<0.001, *****P*<0.0001; unpaired Student's *t*-test with Welch's correction except E (Watson non-parametric two-sample U² test). Scale bars: 5 μm.

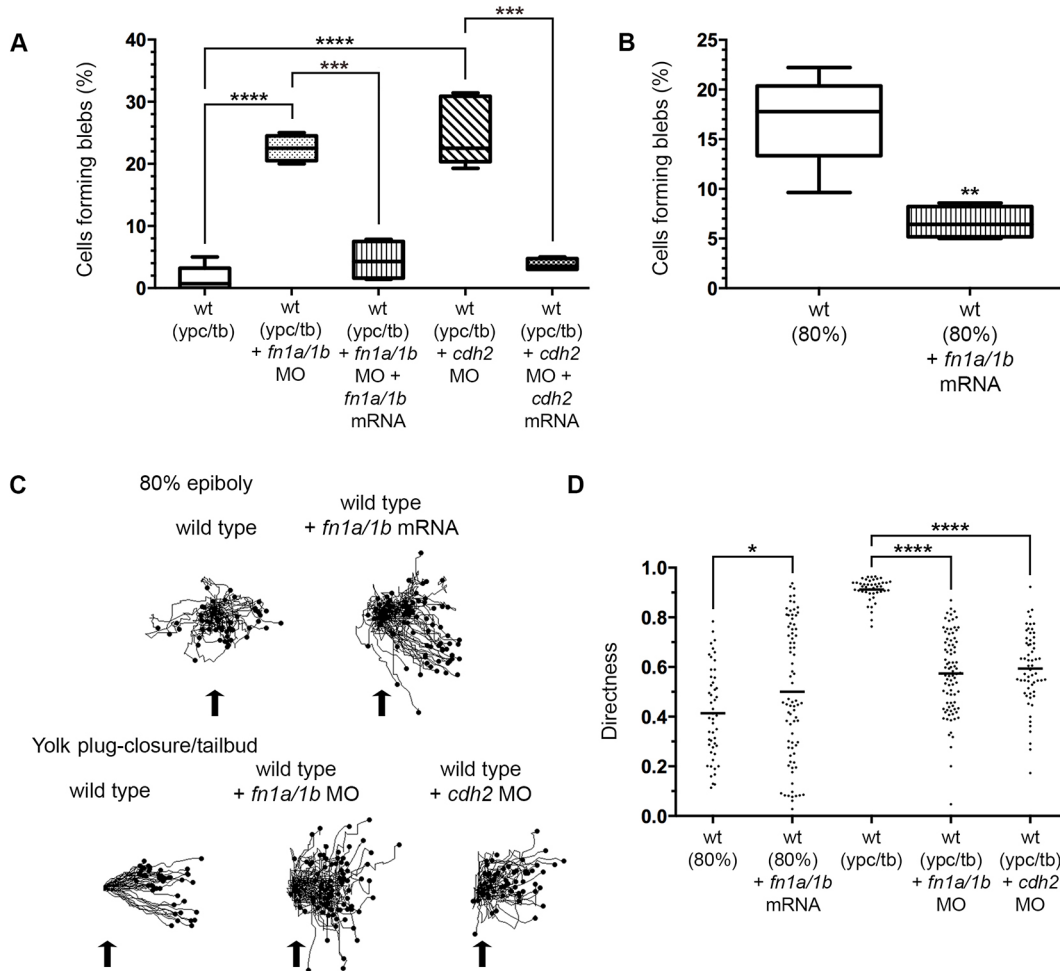


Fig. 6. Fibronectin and Cdh2 suppress bleb formation and promote directed migration. (A) Percentage of cells forming bleb protrusions during the 15 min time-lapse imaging (wild type at *ypc/tb+fn1a/1b* MO, $n=400$ cells, 4 embryos; wild type at *ypc/tb+fn1a/1b* MO+*fn1a/1b* mRNA, $n=140$ cells, 4 embryos; wild type at *ypc/tb+cdh2* MO, $n=840$ cells, 6 embryos; wild type at *ypc/tb+cdh2* MO+*cdh2* mRNA, $n=400$ cells, 4 embryos). (B) Percentage of cells forming blebs (wild type at 80% epiboly+*fn1a/1b* mRNA, $n=560$ cells, 4 embryos). (C) Cell migration tracks toward the dorsal body axis. Origins (black arrows) were standardized for comparison. (D) Directness values for individual cells (wt+*fn1a/1b* mRNA, $n=80$ cells, 3 embryos; wild type+*fn1a/1b* MO, $n=86$ cells, 3 embryos; wild type+*cdh2* MO, $n=60$ cells, 3 embryos). Box plots (A,B) show the interquartile dataset, the median and the data range. Scatter plot (D) shows individual data points and average values. * $P<0.05$, ** $P<0.01$, *** $P<0.001$, **** $P<0.0001$; unpaired Student's *t*-test with Welch's correction.

directness compared with wild type (Fig. 6C,D). Notably, the directness values for mesendodermal cells from *fn1a/1b* mRNA-injected embryos were slightly higher at 80% epiboly (Fig. 6C,D). Together, these data support the notion that bleb protrusions are suppressed at late gastrulation stages due to a combination of cell-matrix and cell-cell interactions. We hypothesize that fibronectin and Cdh2 also promote actin-rich protrusive activity by lateral mesodermal cells.

***vangl2* mutant mesodermal cells have a greater number of bleb protrusions**

At late gastrulation, *vangl2* mutant mesodermal cells resemble mid-gastrulation stage wild-type mesodermal cells because they lack PCP, are less packed and migrate dorsally along indirect trajectories (Jessen et al., 2002; Sepich et al., 2000). Our data suggest there is a correlation between bleb protrusion formation and disrupted PCP in late gastrulation stage lateral mesodermal cells. Moreover, our work has implicated fibronectin as a suppressor of mesendodermal and mesodermal bleb protrusive activity. We therefore analyzed blebbing in *vangl2* mutant embryos and determined whether

manipulation of Ezrb and fibronectin affected *vangl2* phenotypes. Owing to potential differences in embryo staging and lateral position analyzed between published work and our data, we confirmed that mesodermal cells had a PCP phenotype in *vangl2^{vu67/vu67}* mutants (Fig. 7A,B, Figs S1 and S7). We next hypothesized that loss of Vangl2 function would cause greater blebbing at late gastrulation compared with wild type. Our data show that the percentage of *ypc/tb* stage mesodermal cells with blebs was significantly higher in *vangl2* mutants (Fig. 7C, Fig. S5; Movie 11). There was also an increase in the number of blebs per mesodermal cell in *vangl2* mutants (Fig. S6). As our findings suggested a connection between blebbing and disrupted PCP, we next determined whether *ca-ezrb* mRNA injection could rescue *vangl2* phenotypes. We first observed that *ca-ezrb* did not have an appreciable effect on the *vangl2* convergence and extension defect. At the cellular level, however, mesodermal cells in injected *vangl2* mutants continued to show reduced elongation but had partially rescued MLA compared with controls (Fig. 7A,B,D, Figs S5 and S7; Movie 12). Overexpression of *ca-ezrb* also rescued both the blebbing and directed migration phenotypes of *vangl2* mutant cells (Fig. 7C,E,

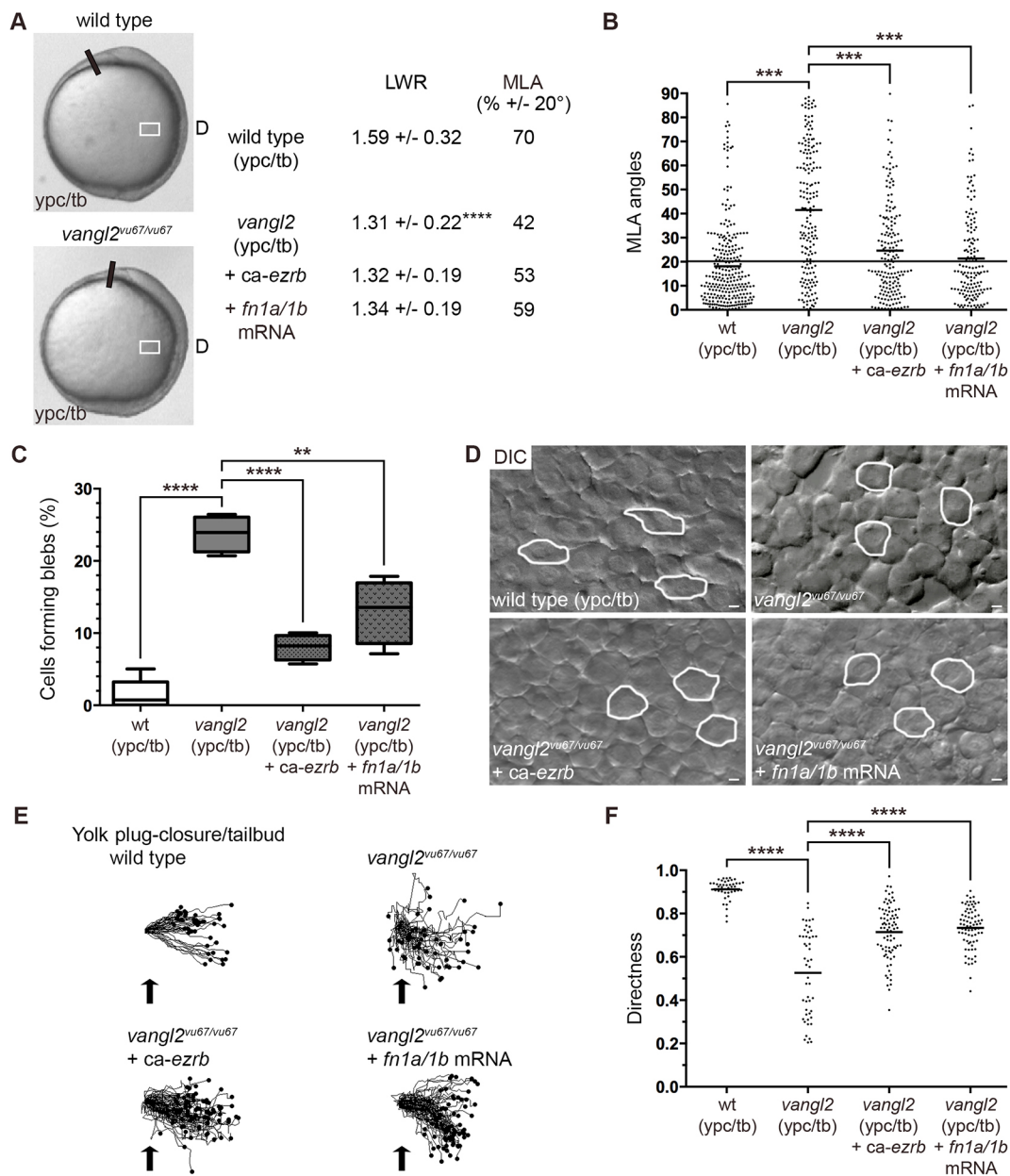


Fig. 7. Loss of *vangl2* causes greater blebbing at late gastrulation. (A) Live control and *vangl2*^{vu67/vu67} mutant embryo images (reproduced from Fig. 2A) at the ypc/tb stage. White boxes indicate approximate position of microscopic analysis. D, dorsal. PCP quantitation of lateral mesodermal cells (*vangl2*^{vu67/vu67}, *n*=180 cells, 4 embryos; *vangl2*^{vu67/vu67}+*ca-ezrb*, *n*=175 cells, 4 embryos; *vangl2*^{vu67/vu67}+*fn1a/1b* mRNA, *n*=150 cells, 3 embryos). (B) MLA data from A depicted as individual data points (in degrees). Long black line indicates 20°. (C) Percentage of cells forming bleb protrusions during the 15 min time-lapse imaging (*vangl2*^{vu67/vu67}, *n*=560 cells, 4 embryos; *vangl2*^{vu67/vu67}+*ca-ezrb*, *n*=560 cells, 4 embryos; *vangl2*^{vu67/vu67}+*fn1a/1b* mRNA, *n*=560 cells, 4 embryos). (D) Live embryo DIC images of lateral mesodermal cells oriented as shown in A and Fig. 2A with dorsal to the right and anterior to the top. Wild-type and *vangl2* mutant images are reproduced from Fig. 1A. Selected cells are outlined to show elongation and alignment relative to the dorsal-ventral body axis. Scale bars: 5 μ m. (E) Cell migration tracks toward the dorsal body axis. Origins (black arrows) were standardized for comparison. (F) Directness values for individual cells (*vangl2*^{vu67/vu67}, *n*=50 cells, 3 embryos; *vangl2*^{vu67/vu67}+*ca-ezrb*, *n*=80 cells, 3 embryos; *vangl2*^{vu67/vu67}+*fn1a/1b* mRNA, *n*=75 cells, 3 embryos). Box plot (C) shows the interquartile dataset, the median and the data range. Scatter plots (B,F) show individual data points and average values. ***P*<0.01, ****P*<0.001, *****P*<0.0001; unpaired Student's *t*-test with Welch's correction except B (Watson non-parametric two-sample *U*² test).

F, Fig. S6). Last, we tested how injection of *fn1a/1b* mRNA affected PCP, blebbing and directed migration in *vangl2* mutant embryos. Similar to *ca-ezrb*, overexpression of fibronectin partially rescued the MLA and bleb protrusion defects in *vangl2* mutant lateral mesodermal cells (Fig. 7A-D, Figs S5 and S7; Movie 13). In addition, *fn1a/1b* mRNA injection improved the migration directness of *vangl2* mutant mesodermal cells (Fig. 7E,F). These results provide evidence that Vangl2 functions to suppress membrane blebbing at late

gastrulation stages. Additionally, our data show that greater blebbing is linked to both the MLA and directed migration defects in *vangl2* mutant mesoderm.

Vangl2 regulates membrane protrusions cell autonomously

Similar to other core PCP genes encoding transmembrane proteins, *vangl2* functions both cell-autonomously and non-autonomously to regulate the elongation and MLA of gastrula cells (Jessen et al.,

2002). In addition to fibronectin and Cdh2, our data now implicate Vangl2 in the control of the membrane-protrusive activity of mesodermal cells. Therefore, we used cell transplantation experiments to create chimeric embryos and determine how *vangl2* regulates blebbing and filopodia in lateral cells. For comparison, we also tested the non-autonomous function of fibronectin. Donor embryos were injected with a combination of Lifeact-GFP, memRFP and, for some experiments, a *vangl2* MO. The *vangl2* MO we used precisely recapitulates the *vangl2* genetic mutant phenotypes at both the embryonic and cellular levels

(Dohn et al., 2013; Love et al., 2018). Host embryos were either uninjected or injected with *vangl2* or *fn1a/1b* MOs. Morphant donor and host phenotypes were confirmed either visually or using immunolabeling (Fig. 8A). Time-lapse confocal imaging was used to track donor cell protrusion formation at late gastrulation (Fig. 8B). We confirmed that, under our experimental conditions, *vangl2* affected PCP in lateral mesodermal cells both cell-autonomously and non-autonomously (Fig. 8C). We next quantified the number of donor cells forming blebs and filopodia during the 15 min time-lapse imaging period. In the first transplantation scheme, we

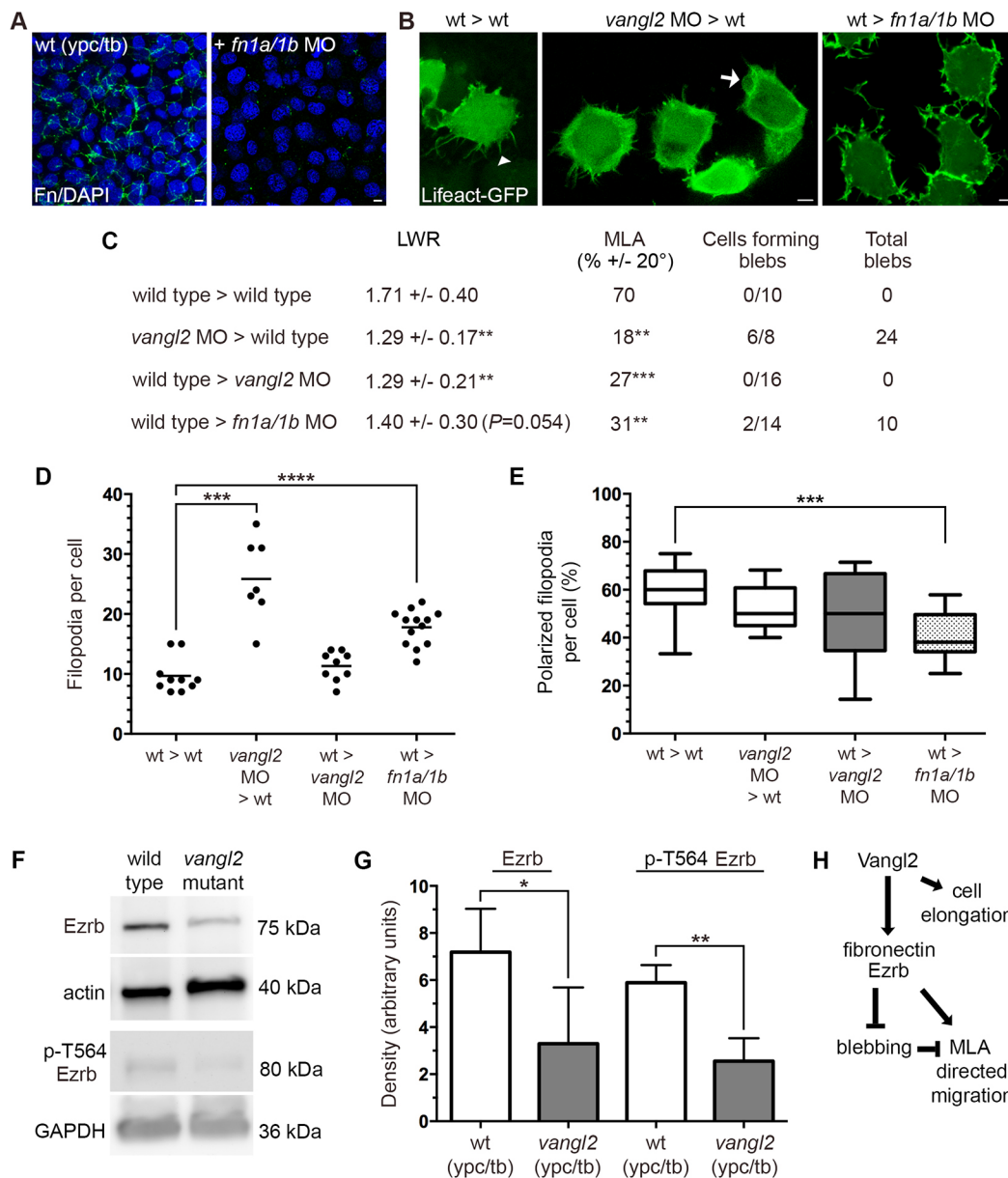


Fig. 8. *vangl2* acts cell-autonomously to regulate bleb protrusive activity. (A) Wild-type control and *fn1a/1b* MO-injected host embryo immunolabeled using a fibronectin (Fn) antibody and stained with DAPI. (B) Lifeact-GFP labeled donor cells transplanted to host embryos (dorsal to the right). White arrowhead marks a single filopodia and white arrow indicates a bleb protrusion. (C) PCP and bleb protrusion quantitation for lateral mesodermal donor cells (wild type>wild type, $n=10$ cells, 5 embryos; *vangl2* MO>wild type, $n=8$ cells, 3 embryos; wild type>*vangl2* MO, $n=16$ cells, 6 embryos; wild type>*fn1a/1b* MO, $n=14$ cells, 4 embryos). (D,E) Donor cell filopodia protrusion number (D) and polarization in relation to the dorsal-ventral body axis (E). (F) Representative western blots of total and phospho-Ezrb (T564) expression in wild-type control and *vangl2*^{vu67/vu67} mutant embryos. (G) Quantitation of western blot band density normalized to β -actin or GAPDH ($n=3$ experimental replicates). (H) Summary diagram of key experimental findings. Scatter plot (D) shows individual data points and average values. Box plot (E) shows the interquartile dataset, the median and the data range. Bar graph (G) shows average values \pm the s.d. * $P<0.05$, ** $P<0.01$, *** $P<0.001$, **** $P<0.0001$; unpaired Student's *t*-test with Welch's correction. Scale bars: 5 μ m.

observed that the wild-type host environment was insufficient to suppress bleb or filopodia formation by *vangl2* morphant donor cells (Fig. 8C,D). In the reverse experiment, we found that wild-type donor cells transplanted to a *vangl2* morphant host did not exhibit abnormal protrusive activity (Fig. 8C,D). Together, these data show that *vangl2* functions cell-autonomously to regulate protrusion formation. In contrast to *vangl2*, loss of fibronectin non-autonomously disrupted protrusion formation and polarity (Fig. 8C-E). As *ezrb* is thought to function cell-autonomously (Diz-Muñoz et al., 2016), we reasoned that Vangl2 may inhibit blebbing by affecting the expression or activation of Ezrb. Western blots were performed using total protein extracts from ypc/tb stage *vangl2* mutant and wild-type control embryos. The data show that ypc/tb stage *vangl2* mutants had significantly reduced levels of both total Ezrb protein and phosphorylated (T564) Ezrb (Fig. 8F,G). We propose that reduced Ezrb protein in *vangl2* mutants at least partly explains the cell-autonomous phenotype.

DISCUSSION

Loss of PCP protein function causes strong convergence and extension phenotypes characterized by defective elongation and MLA of gastrula cell populations (Jessen et al., 2002; Marlow et al., 2002; Topczewski et al., 2001; Xing et al., 2018). These data have provided a broad functional definition for proteins like Vangl2. However, it remains unclear how establishment of PCP relates to formation of membrane protrusions and the overall process of dorsal convergence. We have addressed this question by examining the transition to PCP-dependent cell migration that occurs at late zebrafish gastrulation.

At mid-gastrulation, lateral mesendodermal cells are not packed and migrate dorsally along indirect paths (Jessen et al., 2002). Our data show these cells form actin-rich and bleb membrane protrusions. It was reported that, at early gastrulation, mesendodermal cells engaged in animal pole migration use blebs during tumbling phases, as cells reorient themselves toward the path of movement (Diz-Muñoz et al., 2016). These early gastrula cells seem to depend on polarized actin-rich protrusions during run phases. We find that, similar to germ cells (Reichman-Fried et al., 2004), lateral mesendodermal cells form a large number of polarized blebs as they migrate dorsally (runs). It is known that mid-gastrulation stage wild-type mesendodermal cells exhibit a higher movement velocity compared with late gastrulation (Jessen et al., 2002). Therefore, our data support a model where blebbing is a useful migration strategy at mid-gastrulation stages when little ECM is present (Latimer and Jessen, 2010) and there are a greater number of intercellular gaps. The lack of ECM would support a fast migration mode that is likely integrin independent (Charras and Sahai, 2014). However, our data also showed that inhibition of blebbing at 80% epiboly through *ca-ezrb* or fibronectin mRNA injection was able to promote directed migration of lateral mesendodermal cells. We attribute this to a shift from blebs to actin-rich protrusions, an increase in cell packing and a decrease in cell tumbling (Diz-Muñoz et al., 2016). If mid-gastrulation stage cells are moving dorsally, albeit along indirect paths, why does the migration of late gastrulation mesodermal cells require PCP?

Dorsal convergence involves the movement of a large number of mesodermal cells toward the embryonic body axis. This entails the cells occupying less mediolateral space and becoming increasingly packed. It is for this reason we hypothesize that lateral mesoderm undergoes the transition to PCP-dependent migration. The ability of lateral cells to elongate and mediolaterally align represents an effective mechanism with which to achieve simultaneous packing

and improve directed movement. Bleb-mediated tumbles would not be needed for cell reorientation because packed mesodermal and ectodermal cells are contact inhibited. Knockdown of Ezrb disrupted cell elongation and MLA, suggesting that blebbing and decreased formation of actin-rich protrusions is either directly or indirectly inhibitory to PCP. Our current data (mesoderm) and published findings (ectoderm) (Love et al., 2018) show that lateral gastrula cells do not form a majority of leading edge actin-rich protrusions. We find that mesodermal filopodia have a mediolateral bias, while larger protrusions are not physically polarized. This contrasts with data showing that lateral ectodermal cells have mediolaterally polarized large protrusions but non-polarized filopodia (Love et al., 2018). Future experiments will determine whether protrusion polarity is manifested as differences in protrusion structure, stability or adhesiveness to the ECM and neighboring cells. The significance of bipolar protrusion polarity for lateral gastrula cells is unclear. During mediolateral intercalation, polarized cells use medial and lateral protrusions to generate traction forces by attaching to adjacent cells or the ECM and then shortening (Keller and Shook, 2008). We hypothesize that migrating gastrula cell populations use bipolar protrusions to facilitate MLA and packing. Filopodia in particular are noted for their expression of integrins and cadherins, and an ability to probe the extracellular environment (Jacquemet et al., 2015). For mesodermal cells, filopodia may function to sense fibronectin structure and stiffness or the presence of neighboring cells, and thereby facilitate cell elongation and alignment.

The ECM has a profound effect on cell migration (Charras and Sahai, 2014) and cells are able to respond to changes in cell-matrix adhesion by switching between blebbing and actin-rich protrusions (Tozluoğlu et al., 2013). Ray Keller and colleagues were the first to demonstrate that manipulation of PCP proteins affects organization of the *Xenopus laevis* gastrula fibronectin ECM (Goto et al., 2005). Our data show that manipulation of fibronectin is sufficient to affect bleb formation, PCP and directed migration, suggesting that a positive-feedback loop between PCP signaling and fibronectin regulates gastrulation movements. During gastrulation, the temporal appearance of fibrillar fibronectin beneath deep mesoderm correlates with the onset of PCP. We propose there is a relationship between fibril assembly and reduced blebbing by mesodermal cells. This is supported by our data showing that *fn1a/1b* mRNA injection reduces bleb formation in 80% epiboly stage wild-type cells and late gastrulation stage *vangl2* mutant cells. Increased fibrillogenesis will require one or more integrin $\alpha\beta$ heterodimers capable of binding fibronectin (Schwarzbauer and Sechler, 1999), but although it is clear that PCP requires ECM, the identity of the necessary integrins is unknown. Current data indicate that disruption of integrin $\alpha5$ or αv does not produce a convergence and extension defect, as visualized at the whole embryo level (Dray et al., 2013; Jülich et al., 2009). However, cell culture data suggest that there is regulatory crosstalk between human VANGL2 and integrins αv , $\beta3$ and $\beta5$ (Jessen and Jessen, 2017; Jessen and Jessen, 2019). These reports demonstrate that integrin-ECM interactions are required to maintain VANGL2 protein stability and cell-surface expression. This concept is supported by data showing that loss of zebrafish fibronectin reduces Vangl2 membrane expression in mesoderm and ectoderm (Love et al., 2018).

In addition to matrix adhesion, convergence of the lateral mesoderm involves dynamic changes in cell-cell positioning within the tissue plane and vertical interactions with neighboring cells. Despite strong expression of *cdh2* transcripts in lateral mesoderm, *cdh2* mutations do not produce the severe convergence and

extension phenotypes associated with PCP mutants (Harrington et al., 2007; Lele et al., 2002; Warga and Kane, 2007). Our data indicate that Cdh2 is required to suppress blebbing and promote PCP in mesodermal cells but not in the ectoderm. This contrasts with proteins such as Vangl2 that exhibit widespread expression and control PCP throughout the mesoderm and ectoderm (Jessen et al., 2002). Our findings also show a significant increase in the membrane expression of mesodermal Cdh2 at late gastrulation. It is unclear how Cdh2 regulates bleb formation and whether this is a direct effect. Published data show that downregulation of E-cadherin is required for the onset of germ cell migration and that excess E-cadherin disrupts cell migration speed and bleb protrusion polarity (Blaser et al., 2005; Dzementsei et al., 2013). Another study performed on epiblast cells prior to the onset of gastrulation demonstrated that E-cadherin functions to promote blebbing (Schepis et al., 2012). Cadherin-mediated cell adhesion also exerts mechanotension on the actin cytoskeleton and can influence interactions between integrins and fibronectin (Weber et al., 2011). Therefore, greater bleb formation in *cdh2* morphants and mutants may be partly due to abnormal fibronectin assembly (Dohn et al., 2013).

In *vangl2* mutant embryos, PCP is not established and late gastrulation stage mesodermal cells remain rounder and misaligned, similar to wild-type cells at mid-gastrulation. We report that, together with adhesion proteins, Vangl2 regulates the transition in membrane-protrusive activity that includes both polarization of filopodia and a reduction in bleb protrusion formation. We contend that greater blebbing by *vangl2* mutant late gastrulation mesodermal cells is directly related to defective MLA and directed migration. Injection of *ca-ezrb* or *fn1a/1b* mRNA into *vangl2* mutant embryos suppressed blebbing and partially rescued both cell alignment and directed movement. These data suggest that MLA is a key requirement for effective dorsal convergence. By contrast, the *vangl2* mutant cell elongation defect was not improved by either *ca-ezrb* or *fn1a/1b*. We hypothesize that mediolateral actin-rich protrusions are necessary for cell elongation, and, without these, *ca-ezrb*- or *fn1a/1b*-expressing *vangl2* mutant cells do not achieve a wild-type level of alignment and directed migration. Published findings show that MLA and cell elongation occur concomitantly (Roszko et al., 2015), but that these two processes can be independently regulated (Marlow et al., 2002). It is notable that neither *ca-ezrb* nor *fn1a/1b* suppressed the *vangl2* convergence and extension phenotype. As mentioned, wild-type lateral ectodermal cells form few blebs, and ectodermal blebbing is not greater in *vangl2* mutants (Love et al., 2018). Therefore, *ca-ezrb* or *fn1a/1b* mRNA injection is unlikely to influence the ectodermal PCP defect in *vangl2* mutant embryos.

How does Vangl2 regulate mesodermal cell protrusions? In migrating zebrafish cells, Vangl2 protein expression is detected in polarized and non-polarized larger actin-rich protrusions (Love et al., 2018) and filopodia (Davey et al., 2016). These reports suggest that Vangl2 is enriched in protrusions compared with non-protrusive membrane domains (Love et al., 2018) and may function to destabilize protrusions (Davey et al., 2016). Our cell transplantation experiments showed that *vangl2* acts cell-autonomously to regulate bleb and filopodia formation. Despite having higher matrix metalloproteinase activity and reduced fibronectin (Dohn et al., 2013; Williams et al., 2012), *vangl2* morphant host embryos failed to exert a non-autonomous effect on filopodia number or polarity. This may be because, unlike fibronectin knockdown, *vangl2* morphants and germline mutants retain a modest level of fibrillar fibronectin. Vangl2 may regulate

additional aspects of protrusion dynamics in a non-autonomous fashion. For motor neurons, *vangl2* acts non-autonomously to regulate protrusion stability (Davey et al., 2016). We show that *vangl2* mutant embryos have significant reductions in the levels of total and activated Ezrb protein. This finding supports the notion that *vangl2* acts cell-autonomously to promote blebbing by disrupting Ezrb expression and weakening membrane adhesion to cortical actin. It is unclear how Vangl2 controls Ezrb protein levels and whether this represents a direct effect. We hypothesize that Vangl2 regulates Ezrb via Rho-associated coiled-coil containing protein kinase (Rock). Rock activates myosin II to promote actomyosin contractility and both bleb initiation and retraction (Charras and Paluch, 2008). Rock can also phosphorylate and activate ezrin (Matsui et al., 1998). Rock2a has been shown to regulate PCP and directed gastrula cell migration, and limited data suggest Vangl2 may function to stabilize Rock2a at the plasma membrane (Jessen et al., 2002; Marlow et al., 2002), possibly by affecting RhoA expression (Phillips et al., 2005).

In conclusion, our data establish that the onset of PCP in lateral mesoderm requires a transition in membrane-protrusive activity that is dependent on Vangl2 and the cell-adhesion proteins fibronectin and Cdh2 (Fig. 8H). At mid-gastrulation, when little ECM is present and migrating mesodermal cells are not packed, bleb protrusions provide a mechanism for both rapid movement (runs) and reorientation followed by course correction (tumbles). By late gastrulation, as cell packing and fibrillar fibronectin levels increase, mesodermal cells use actin-rich protrusions as they engage in directed migration. We propose that Vangl2-dependent formation and polarization of filopodia underlies PCP establishment and cell cohesion. In addition, by increasing Ezrb protein levels Vangl2 inhibits blebbing and promotes PCP and directed migration. Future work will determine more precisely how Vangl2 regulates actin-rich protrusions and dorsal convergence, and further define the roles of cell-matrix and cell-cell adhesion. We are particularly interested in crosstalk between these processes and both actomyosin contractility and cellular mechanotension.

MATERIALS AND METHODS

Zebrafish husbandry and genetic strains

Wild-type (AB, TL and WIK), *vangl2^{vu67/+}* (Roszko et al., 2015) and *vangl2^{m209/+}* (Solnica-Krezel et al., 1996) adult zebrafish (*Danio rerio*) were maintained using standard procedures (Solnica-Krezel et al., 1994). Embryos collected after natural spawnings were grown in egg water (60 mg/l Instant Ocean in reverse osmosis water) and staged according to their morphology (Kimmel et al., 1995). The *vangl2^{vu67}*, *vangl2^{m209}* and *cdh2^{m101/m101}* alleles are homozygous recessive null loss-of-function mutations (Jessen et al., 2002; Lele et al., 2002; Roszko et al., 2015). The Middle Tennessee State University Institutional Animal Care and Use Committee approved this research and all procedures were conducted using approved guidelines (Office of Laboratory Animal Welfare assurance number A4701-01).

Embryo microinjection

Microinjection of one-cell-stage or 16-cell-stage embryos was performed using standard methods (Gilmour et al., 2002). The DNA constructs, the procedure for making synthetic mRNA and the injection doses (Lifeact-GFP, memRFP, *fn1a* and *fn1b*) have been described previously (Love et al., 2018). Linearized template DNA was purified using phenol:chloroform extraction followed by ethanol precipitation. Given the ~7.2 kb length of the *fn1a* and *fn1b* transcripts, 1 µl of 20 mM GTP was added to the transcription reactions as directed by the manufacturer (mMessage mMachine, Ambion). The *ca-ezrb* DNA construct has been previously published (Gautreau et al., 2000). Full-length *cdh2* was cloned in pCS2⁺ vector. Synthetic mRNAs were generated after NotI linearization using Sp6 RNA polymerase and

mRNAs injected at a concentration of ~150 pg/embryo. Antisense MO oligonucleotides were acquired from Gene Tools and suspended in distilled water. The *ezrb*, *fn1a*, *fn1b*, *cdh2* and *vangl2* MO sequences and injection doses have been described previously (Dohn et al., 2013; Jülich et al., 2005; Latimer and Jessen, 2010; Lele et al., 2002; Link et al., 2006; Love et al., 2018). None of these MOs cause obvious p53-mediated cell death in injected embryos. Western blots were performed on protein extracts from *ezrb* and *cdh2* MO-injected embryos (Fig. S9).

Whole-mount *in situ* hybridization, western blotting and immunofluorescence

We performed whole-mount *in situ* hybridization as previously described (Love et al., 2018) using an antisense RNA probe that recognizes protocadherin 8 (Yamamoto et al., 1998). Embryo whole-cell lysates were prepared and analyzed by western blotting as described previously (Love et al., 2018). The following antibodies were used: moesin (1:500, 610401, BD Transduction Laboratory), T567 phospho-ezrin (1:500, 3141, Cell Signaling Technology), β -actin (1:1000, 4967, Cell Signaling Technology), GAPDH (1:1000, AM4300, Ambion) and pan-cadherin (1:1000, AB16505, Abcam). Peroxidase-conjugated secondary antibodies were used at 1:5000 (Jackson ImmunoResearch). Western blot band density was quantified using UVP Visionworks software. Immunolabeling was performed after fixation with Prefer (Anatech) for 2 h at room temperature as described previously (Love et al., 2018). Antibodies used for immunofluorescence included pan-cadherin (1:100) and fibronectin (1:100, F3648, Millipore-Sigma). Fluorophore-conjugated secondary antibodies were used at 1:500 (Jackson ImmunoResearch). Embryos were incubated for 30 min with DAPI [2-(4-amidinophenyl)-1H-indole-6-carboxamide] to label nuclei followed by PBS washing. Pan-cadherin localization was quantified using Fiji's Plot Profile tool to determine fluorescence intensities along lines drawn across the plasma membranes of adjacent cells.

DIC and confocal imaging

Live and fixed embryos were mounted in agarose on coverslip dishes as previously described (Jessen, 2012). Confocal imaging was carried out using an inverted Zeiss Axio Observer LSM700 laser-scanning confocal microscope and a 63 \times oil-immersion objective (N.A. 1.4). The *z*-axis step size was 0.5 μ m for all confocal analysis. DIC imaging was carried out using an inverted Olympus IX83 microscope equipped with a 40 \times air-objective (N.A. 0.95) and a Hamamatsu Flash 4.0 CMOS camera. A Coded Intermediate Magnification Changer (IX3-CAS) was used at 1.6 \times to enhance visualization of blebs with DIC. For both confocal and DIC imaging, low-magnification (10 \times) transmitted light reference pictures were taken to confirm embryo orientation and notochord position. Live ypc/tb stage embryo images were obtained using an Olympus SZX16 stereomicroscope equipped with an Olympus Q-Color5 CCD camera.

Quantitation of PCP, directed migration and membrane protrusions

PCP (cell elongation and MLA) was quantified from DIC and confocal time-lapse images taken from live embryos using Fiji software (fiji.sc) (Schindelin et al., 2012) as described previously (Jessen, 2012). Cell migration directionality data were obtained by tracking individual cell movements from time-lapse videos using Fiji's Manual Tracking tool. These data were exported to Ibidi's Chemotaxis and Migration Tool standalone software (ibidi.com) to generate directness values and cell plot diagrams. To analyze actin-rich membrane protrusions using confocal microscopy, 16-cell-stage embryos were injected to achieve mosaic expression of Lifeact-GFP. Fluorescent time-lapse images were collected at 28°C for 15 min with 1 min sampling intervals. Protrusions were identified as filopodia or larger protrusions as described previously (Love et al., 2018). Membrane spikes less than 1.5 μ m in length were excluded from our analyses because of their short half-life. DIC time-lapse imaging of bleb protrusions was also carried out at 28°C for 15 min with 30 s sampling intervals. Mesendodermal cells were classified as being in phases of 'runs' or 'tumbles', essentially as defined for early gastrula cells (Diz-Muñoz et al., 2016). Cells in the 'run' phase were actively making forward progress

during multiple imaging frames, whereas cells in the 'tumble' phase did not show directed movement. The polarity of actin-rich and bleb protrusions was analyzed using Fiji's Angle tool. Mesodermal cell protrusion polarity was determined in relation to the dorsal embryonic body axis (Fig. S1). Mesendodermal cell bleb protrusion polarity during runs and tumbles was quantified in relation to the meandering path of dorsal movement (Fig. S1). Protrusions formed at angles $\pm 45^\circ$ were considered to be polarized.

Cell transplantation

Transplantation of cells between donor and host embryos was achieved following standard methods (Jessen et al., 2002; Roszko et al., 2015). Donor embryos were injected at the one-cell stage with *vangl2* MO and/or Lifeact-GFP and memRFP. Host embryos were either not injected or injected at the one-cell stage with *vangl2* or *fn1a/1b* MOs. Donor embryos were allowed to develop at 28.5°C until sphere stage. Approximately 50-100 donor cells were transplanted into the margin of host embryos at 50% epiboly using an IM-11-2 pneumatic microinjector (Narishige) and 1 mm capillary needles without filament (TW100-4, World Precision Instruments). Confocal time-lapse imaging of lateral mesodermal donor cells was performed at the ypc/tb stage as described above.

Transmission electron microscopy

Wild-type and *vangl2*^{m209/m209} mutant embryos were fixed at the ypc/tb stage with 2.5% glutaraldehyde in 0.1 M cacodylate buffer. After being dechorionated, embryos were processed for TEM following standard procedures (Rieger and Koster, 2007). Thicker cross-sections (500 nm) were used to verify embryo orientation prior to making thinner sections (~80 nm). Images were obtained using a Philips/FEI T-12 microscope equipped with a 2k by 2k CCD camera system.

Statistics

Data were assembled in Microsoft Excel and exported to Prism8 (GraphPad) or VectorRose for graphing and statistical analyses. For the Watson U² statistical test, critical values greater than 0.187, 0.268 and 0.385 were considered significant at 0.05, 0.01 and 0.001 levels, respectively (Zar, 2009). The type of statistical test performed and the resulting significance values are noted in the figures and legends, as are the numbers of cells and embryos analyzed for each experiment. The data presented have a normal distribution.

Acknowledgements

We thank Tammy Jessen and Denise Ortega for excellent zebrafish care, and Alba Diz-Muñoz and Martin Bergert for the *ca-ezrb* plasmid.

Competing interests

The authors declare no competing or financial interests.

Author contributions

Conceptualization: J.R.J.; Methodology: D.J.P., J.R.J.; Validation: D.J.P., J.R.J.; Formal analysis: D.J.P., J.R.J.; Investigation: D.J.P.; Resources: J.R.J.; Writing - original draft: D.J.P., J.R.J.; Writing - review & editing: D.J.P., J.R.J.; Visualization: D.J.P., J.R.J.; Supervision: J.R.J.; Project administration: J.R.J.; Funding acquisition: J.R.J.

Funding

This study was funded by a grant from the National Institutes of Health (GM102356 to J.R.J.). Some equipment items were provided by Middle Tennessee State University. J.R.J. and D.J.P. acknowledge support from the Molecular Biosciences PhD Program and the Department of Biology. Deposited in PMC for release after 12 months.

Supplementary information

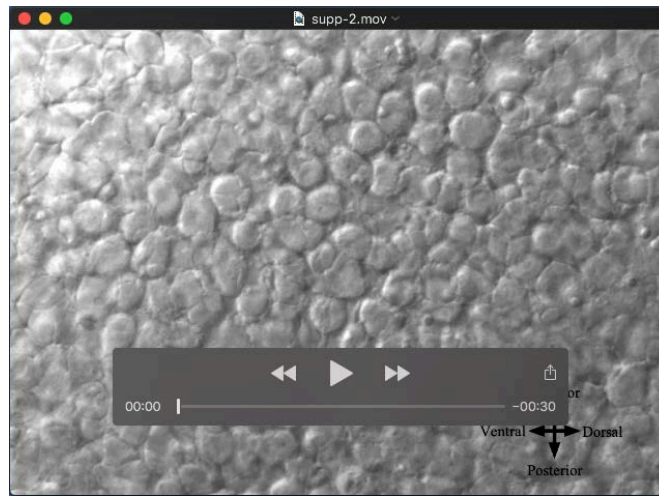
Supplementary information available online at <http://dev.biologists.org/lookup/doi/10.1242/dev.182188.supplemental>

References

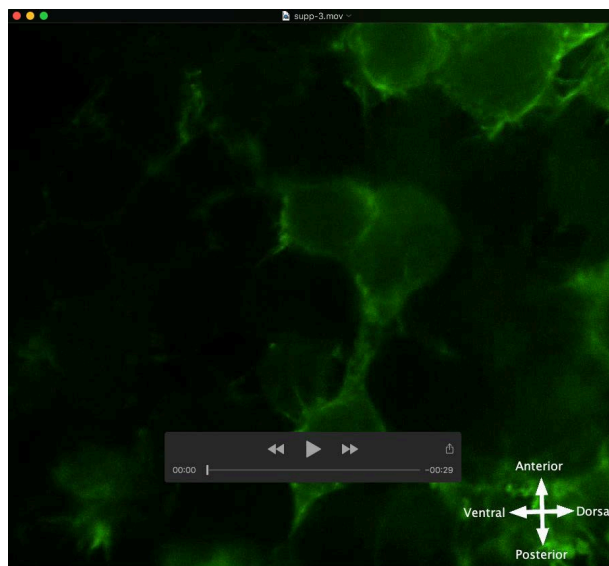
Blaser, H., Eisenbeiss, S., Neumann, M., Reichman-Fried, M., Thisse, B., Thisse, C. and Raz, E. (2005). Transition from non-motile behaviour to directed migration during early PGC development in zebrafish. *J. Cell Sci.* **118**, 4027-4038. doi:10.1242/jcs.02522

- Blaser, H., Reichman-Fried, M., Castanon, I., Dumstrei, K., Marlow, F. L., Kawakami, K., Solnica-Krezel, L., Heisenberg, C.-P. and Raz, E. (2006). Migration of zebrafish primordial germ cells: a role for myosin contraction and cytoplasmic flow. *Dev. Cell* **11**, 613-627. doi:10.1016/j.devcel.2006.09.023
- Bretscher, A., Reczek, D. and Berrymann, M. (1997). Ezrin: a protein requiring conformational activation to link microfilaments to the plasma membrane in the assembly of cell surface structures. *J. Cell Sci.* **110**, 3011-3018.
- Charras, G. and Paluch, E. (2008). Blebs lead the way: how to migrate without lamellipodia. *Nat. Rev. Mol. Cell Biol.* **9**, 730-736. doi:10.1038/nrm2453
- Charras, G. and Sahai, E. (2014). Physical influences of the extracellular environment on cell migration. *Nat. Rev. Mol. Cell Biol.* **15**, 813-824. doi:10.1038/nrm3897
- Davey, C. F., Mathewson, A. W. and Moens, C. B. (2016). PCP signaling between migrating neurons and their planar-polarized neuroepithelial environment controls filopodial dynamics and directional migration. *PLoS Genet.* **12**, e1005934. doi:10.1371/journal.pgen.1005934
- Diz-Muñoz, A., Krieg, M., Bergert, M., Ibarlucea-Benitez, I., Muller, D. J., Paluch, E. and Heisenberg, C.-P. (2010). Control of directed cell migration in vivo by membrane-to-cortex attachment. *PLoS Biol.* **8**, e1000544. doi:10.1371/journal.pbio.1000544
- Diz-Muñoz, A., Romanczuk, P., Yu, W., Bergert, M., Ivanovitch, K., Salbreux, G., Heisenberg, C.-P. and Paluch, E. K. (2016). Steering cell migration by alternating blebs and actin-rich protrusions. *BMC Biol.* **14**, 74. doi:10.1186/s12915-016-0294-x
- Dohn, M. R., Mundell, N. A., Sawyer, L. M., Dunlap, J. A. and Jessen, J. R. (2013). Planar cell polarity proteins differentially regulate extracellular matrix organization and assembly during zebrafish gastrulation. *Dev. Biol.* **383**, 39-51. doi:10.1016/j.ydbio.2013.08.027
- Dray, N., Lawton, A., Nandi, A., Jülich, D., Emonet, T. and Holley, S. A. (2013). Cell-fibronectin interactions propel vertebrate trunk elongation via tissue mechanics. *Curr. Biol.* **23**, 1335-1341. doi:10.1016/j.cub.2013.05.052
- Dzamba, B. J., Jakab, K. R., Marsden, M., Schwartz, M. A. and DeSimone, D. W. (2009). Cadherin adhesion, tissue tension, and noncanonical Wnt signaling regulate fibronectin matrix organization. *Dev. Cell* **16**, 421-432. doi:10.1016/j.devcel.2009.01.008
- Dzementsei, A., Schneider, D., Janshoff, A. and Pieler, T. (2013). Migratory and adhesive properties of *Xenopus laevis* primordial germ cells in vitro. *Biol. Open* **2**, 1279-1287. doi:10.1242/bio.20135140
- Fackler, O. T. and Grosse, R. (2008). Cell motility through plasma membrane blebbing. *J. Cell Biol.* **181**, 879-884. doi:10.1083/jcb.200802081
- Friedl, P. and Gilmour, D. (2009). Collective cell migration in morphogenesis, regeneration and cancer. *Nat. Rev. Mol. Cell Biol.* **10**, 445-457. doi:10.1038/nrm2720
- Gautreau, A., Louvard, D. and Arpin, M. (2000). Morphogenic effects of ezrin require a phosphorylation-induced transition from oligomers to monomers at the plasma membrane. *J. Cell Biol.* **150**, 193-204. doi:10.1083/jcb.150.1.193
- Gilmour, D. T., Jessen, J. R. and Lin, S. (2002). Manipulating gene expression in the zebrafish. In *Zebrafish, a Practical Approach*, Vol. 261 (ed. C. Nusslein-Volhard and R. Dahm), pp. 121-143. New York: Oxford University Press.
- Goto, T., Davidson, L., Asashima, M. and Keller, R. (2005). Planar cell polarity genes regulate polarized extracellular matrix deposition during frog gastrulation. *Curr. Biol.* **15**, 787-793. doi:10.1016/j.cub.2005.03.040
- Harrington, M. J., Hong, E., Fasanmi, O. and Brewster, R. (2007). Cadherin-mediated adhesion regulates posterior body formation. *BMC Dev. Biol.* **7**, 130. doi:10.1186/1471-213X-7-130
- Jacquemet, G., Hamidi, H. and Ivaska, J. (2015). Filopodia in cell adhesion, 3D migration and cancer cell invasion. *Curr. Opin. Cell Biol.* **36**, 23-31. doi:10.1016/jceb.2015.06.007
- Jayasundar, J. J., Ju, J. H., He, L., Liu, D., Meilleur, F., Zhao, J., Callaway, D. J. E. and Bu, Z. (2012). Open conformation of ezrin bound to phosphatidylinositol 4,5-bisphosphate and to F-actin revealed by neutron scattering. *J. Biol. Chem.* **287**, 37119-37133. doi:10.1074/jbc.M112.380972
- Jessen, J. R. (2012). Analyzing planar cell polarity during zebrafish gastrulation. *Methods Mol. Biol.* **839**, 69-78. doi:10.1007/978-1-61779-510-7_6
- Jessen, T. N. and Jessen, J. R. (2017). VANGL2 interacts with integrin α 5 to regulate matrix metalloproteinase activity and cell adhesion to the extracellular matrix. *Exp. Cell Res.* **361**, 265-276. doi:10.1016/j.yexcr.2017.10.026
- Jessen, T. N. and Jessen, J. R. (2019). VANGL2 protein stability is regulated by integrin α 5 and the extracellular matrix. *Exp. Cell Res.* **374**, 128-139. doi:10.1016/j.yexcr.2018.11.017
- Jessen, J. R. and Solnica-Krezel, L. (2005). Morphogenetic cell movements shaping the zebrafish gastrula. In *Planar Cell Polarization During Development*, Vol. 14 (ed. M. Mlodzik), pp. 131-165. San Diego: Elsevier Press. doi:10.1016/S1574-3349(05)14007-1
- Jessen, J. R., Topczewski, J., Bingham, S., Sepich, D. S., Marlow, F., Chandrasekhar, A. and Solnica-Krezel, L. (2002). Zebrafish trilobite identifies new roles for Strabismus in gastrulation and neuronal movements. *Nat. Cell Biol.* **4**, 610-615. doi:10.1038/nmc828
- Jülich, D., Geisler, R. and Holley, S. A. (2005). Integrin α 5 and delta/notch signaling have complementary spatiotemporal requirements during zebrafish somitogenesis. *Dev. Cell* **8**, 575-586. doi:10.1016/j.devcel.2005.01.016
- Jülich, D., Mould, A. P., Koper, E. and Holley, S. A. (2009). Control of extracellular matrix assembly along tissue boundaries via Integrin and Eph/Ephrin signaling. *Development* **136**, 2913-2921. doi:10.1242/dev.038935
- Keller, R. (2002). Shaping the vertebrate body plan by polarized embryonic cell movements. *Science* **298**, 1950-1954. doi:10.1126/science.1079478
- Keller, R. and Shook, D. (2008). Dynamic determinations: patterning the cell behaviours that close the amphibian blastopore. *Philos. Trans. R. Soc. Lond. B Biol. Sci.* **363**, 1317-1332. doi:10.1098/rstb.2007.2250
- Kimmel, C. B., Ballard, W. W., Kimmel, S. R., Ullmann, B. and Schilling, T. F. (1995). Stages of embryonic development of the zebrafish. *Dev. Dyn.* **203**, 253-310. doi:10.1002/aja.1002030302
- Latimer, A. and Jessen, J. R. (2010). Extracellular matrix assembly and organization during zebrafish gastrulation. *Matrix Biol.* **29**, 89-96. doi:10.1016/j.matbio.2009.10.002
- Lele, Z., Folchert, A., Concha, M., Rauch, G. J., Geisler, R., Rosa, F., Wilson, S. W., Hammerschmidt, M. and Bally-Cuif, L. (2002). Parachute/n-cadherin is required for morphogenesis and maintained integrity of the zebrafish neural tube. *Development* **129**, 3281-3294.
- Lin, S., Baye, L. M., Westfall, T. A. and Slusarski, D. C. (2010). Wnt5b-Ryk pathway provides directional signals to regulate gastrulation movement. *J. Cell Biol.* **190**, 263-278. doi:10.1083/jcb.200912128
- Link, V., Carvalho, L., Castanon, I., Stockinger, P., Shevchenko, A. and Heisenberg, C. P. (2006). Identification of regulators of germ layer morphogenesis using proteomics in zebrafish. *J. Cell Sci.* **119**, 2073-2083. doi:10.1242/jcs.02928
- Love, A. M., Prince, D. J. and Jessen, J. R. (2018). Vangl2-dependent regulation of membrane protrusions and directed migration requires a fibronectin extracellular matrix. *Development* **145**, dev165472. doi:10.1242/dev.165472
- Marlow, F., Topczewski, J., Sepich, D. and Solnica-Krezel, L. (2002). Zebrafish Rho kinase 2 acts downstream of Wnt11 to mediate cell polarity and effective convergence and extension movements. *Curr. Biol.* **12**, 876-884. doi:10.1016/S0960-9822(02)00864-3
- Matsui, T., Maeda, M., Doi, Y., Yonemura, S., Amano, M., Kaibuchi, K., Tsukita, S. and Tsukita, S. (1998). Rho-kinase phosphorylates COOH-terminal threonines of ezrin/radixin/moesin (ERM) proteins and regulates their head-to-tail association. *J. Cell Biol.* **140**, 647-657. doi:10.1083/jcb.140.3.647
- Mishra, A. K., Mondo, J. A., Campanale, J. P. and Montell, D. J. (2019). Coordination of protrusion dynamics within and between collectively migrating border cells by myosin II. *Mol. Biol. Cell* **30**, 2490-2502. doi:10.1091/mbc.E19-02-0124
- Phillips, H. M., Murdoch, J. N., Chaudhry, B., Copp, A. J. and Henderson, D. J. (2005). Vangl2 acts via RhoA signaling to regulate polarized cell movements during development of the proximal outflow tract. *Circ. Res.* **96**, 292-299. doi:10.1161/01.RES.0000154912.08695.88
- Reichman-Fried, M., Minina, S. and Raz, E. (2004). Autonomous modes of behavior in primordial germ cell migration. *Dev. Cell* **6**, 589-596. doi:10.1016/S1534-5807(04)00074-7
- Riedl, J., Crevenna, A. H., Kessenbrock, K., Yu, J. H., Neukirchen, D., Bista, M., Bradke, F., Jenne, D., Holak, T. A., Werb, Z. et al. (2008). Lifeact: a versatile marker to visualize F-actin. *Nat. Methods* **5**, 605-607. doi:10.1038/nmeth.1220
- Rieger, S. and Koster, R. W. (2007). Preparation of zebrafish embryos for transmission electron microscopy. *CSH Protoc* **2007**, pdb prot4772. doi:10.1101/pdb.prot4772
- Rozko, I., Sawada, A. and Solnica-Krezel, L. (2009). Regulation of convergence and extension movements during vertebrate gastrulation by the Wnt/PCP pathway. *Semin. Cell Dev. Biol.* **20**, 986-997. doi:10.1016/j.semdb.2009.09.004
- Rozko, I., Sepich, D. S., Jessen, J. R., Chandrasekhar, A. and Solnica-Krezel, L. (2015). A dynamic intracellular distribution of Vangl2 accompanies cell polarization during zebrafish gastrulation. *Development* **142**, 2508-2520. doi:10.1242/dev.119032
- Schepis, A., Sepich, D. and Nelson, W. J. (2012). α E-catenin regulates cell-cell adhesion and membrane blebbing during zebrafish epiboly. *Development* **139**, 537-546. doi:10.1242/dev.073932
- Schindelin, J., Arganda-Carreras, I., Frise, E., Kaynig, V., Longair, M., Pietzsch, T., Preibisch, S., Rueden, C., Saalfeld, S., Schmid, B. et al. (2012). Fiji: an open-source platform for biological-image analysis. *Nat. Methods* **9**, 676-682. doi:10.1038/nmeth.2019
- Schwarzbauer, J. E. and Sechler, J. L. (1999). Fibronectin fibrillogenesis: a paradigm for extracellular matrix assembly. *Curr. Opin. Cell Biol.* **11**, 622-627. doi:10.1016/S0955-0674(99)00017-4
- Sepich, D. S., Myers, D. C., Short, R., Topczewski, J., Marlow, F. and Solnica-Krezel, L. (2000). Role of the zebrafish trilobite locus in gastrulation movements of convergence and extension. *Genesis* **27**, 159-173. doi:10.1002/1526-968X(200008)27:4<159::AID-GENE50>3.0.CO;2-T
- Sepich, D. S., Calmelet, C., Kiskowski, M. and Solnica-Krezel, L. (2005). Initiation of convergence and extension movements of lateral mesoderm during zebrafish gastrulation. *Dev. Dyn.* **234**, 279-292. doi:10.1002/dvdy.20507
- Solnica-Krezel, L. (2005). Conserved patterns of cell movements during vertebrate gastrulation. *Curr. Biol.* **15**, R213-R228. doi:10.1016/j.cub.2005.03.016
- Solnica-Krezel, L., Schier, A. F. and Driever, W. (1994). Efficient recovery of ENU-induced mutations from the zebrafish germline. *Genetics* **136**, 1401-1420.

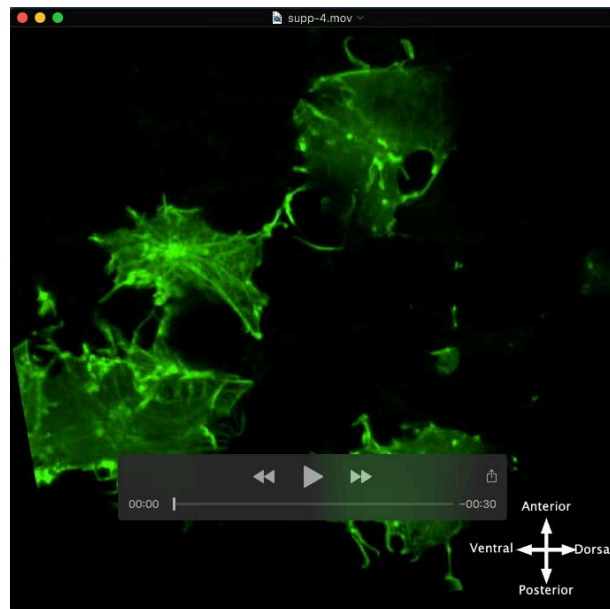
- Solnica-Krezel, L., Stemple, D. L., Mountcastle-Shah, E., Rangini, Z., Neuhauss, S. C., Malicki, J., Schier, A. F., Stainier, D. Y., Zwartkruis, F., Abdelilah, S. et al.** (1996). Mutations affecting cell fates and cellular rearrangements during gastrulation in zebrafish. *Development* **123**, 67-80.
- Topczewski, J., Sepich, D. S., Myers, D. C., Walker, C., Amores, A., Lele, Z., Hammerschmidt, M., Postlethwait, J. and Solnica-Krezel, L.** (2001). The zebrafish glypican knypek controls cell polarity during gastrulation movements of convergent extension. *Dev. Cell* **1**, 251-264. doi:10.1016/S1534-5807(01)00005-3
- Tozluoğlu, M., Tournier, A. L., Jenkins, R. P., Hooper, S., Bates, P. A. and Sahai, E.** (2013). Matrix geometry determines optimal cancer cell migration strategy and modulates response to interventions. *Nat. Cell Biol.* **15**, 751-762. doi:10.1038/ncb2775
- Trinkaus, J. P., Trinkaus, M. and Fink, R. D.** (1992). On the convergent cell movements of gastrulation in *Fundulus*. *J. Exp. Zool.* **261**, 40-61. doi:10.1002/jez.1402610107
- von der Hardt, S., Bakkers, J., Inbal, A., Carvalho, L., Solnica-Krezel, L., Heisenberg, C. P. and Hammerschmidt, M.** (2007). The Bmp gradient of the zebrafish gastrula guides migrating lateral cells by regulating cell-cell adhesion. *Curr. Biol.* **17**, 475-487. doi:10.1016/j.cub.2007.02.013
- Warga, R. M. and Kane, D. A.** (2007). A role for N-cadherin in mesodermal morphogenesis during gastrulation. *Dev. Biol.* **310**, 211-225. doi:10.1016/j.ydbio.2007.06.023
- Weber, G. F., Bjerke, M. A. and DeSimone, D. W.** (2011). Integrins and cadherins join forces to form adhesive networks. *J. Cell Sci.* **124**, 1183-1193. doi:10.1242/jcs.064618
- Williams, M. L. K. and Solnica-Krezel, L.** (2017). Regulation of gastrulation movements by emergent cell and tissue interactions. *Curr. Opin. Cell Biol.* **48**, 33-39. doi:10.1016/j.ccb.2017.04.006
- Williams, B. B., Cantrell, V. A., Mundell, N. A., Bennett, A. C., Quick, R. E. and Jessen, J. R.** (2012). VANGL2 regulates membrane trafficking of MMP14 to control cell polarity and migration. *J. Cell Sci.* **125**, 2141-2147. doi:10.1242/jcs.097964
- Williams, M. L. K., Sawada, A., Budine, T., Yin, C., Gontarz, P. and Solnica-Krezel, L.** (2018). Gon4l regulates notochord boundary formation and cell polarity underlying axis extension by repressing adhesion genes. *Nat. Commun.* **9**, 1319. doi:10.1038/s41467-018-03715-w
- Xing, Y.-Y., Cheng, X.-N., Li, Y.-L., Zhang, C., Saquet, A., Liu, Y.-Y., Shao, M. and Shi, D. L.** (2018). Mutational analysis of dishevelled genes in zebrafish reveals distinct functions in embryonic patterning and gastrulation cell movements. *PLoS Genet.* **14**, e1007551. doi:10.1371/journal.pgen.1007551
- Yamamoto, A., Amacher, S. L., Kim, S. H., Geissert, D., Kimmel, C. B. and De Robertis, E. M.** (1998). Zebrafish paraxial protocadherin is a downstream target of spadetail involved in morphogenesis of gastrula mesoderm. *Development* **125**, 3389-3397.
- Zar, J. H.** (2009). *Biostatistical Analysis*. London: Pearson.



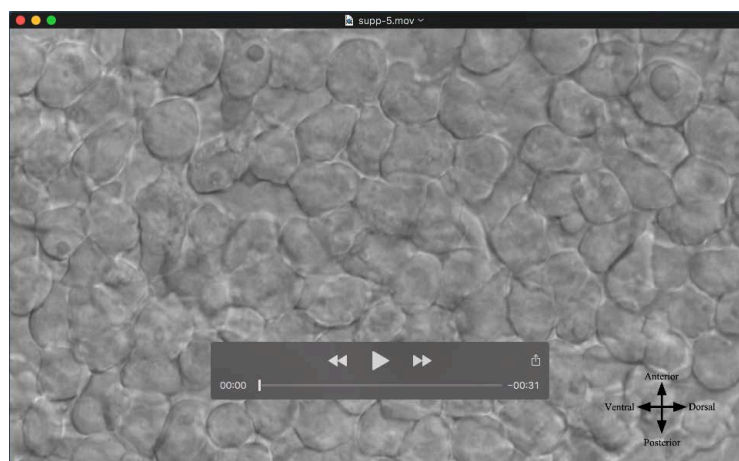
Movie 1. The onset of dorsal convergence. DIC time-lapse imaging of wild-type lateral hypoblast/mesendodermal cells located 90° from the notochord and near the embryo equator as shown in Fig. 2A (15 min time-lapse/30 s imaging intervals). Anterior is to the top and dorsal to the right. At the beginning of imaging, the embryo is at approximately the 75% epiboly stage. The cells initially migrate anteriorly and then make an abrupt right turn toward the dorsal body axis.



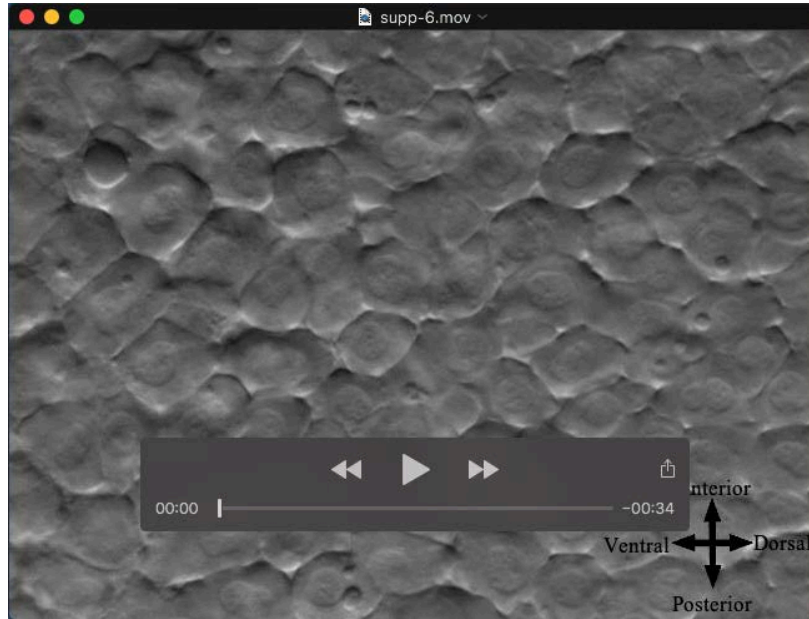
Movie 2. Wild-type embryo + Lifeact-GFP mRNA at 80% epiboly. Confocal time-lapse imaging of hypoblast/mesendodermal cells located 90° from the notochord and near the embryo equator as shown in Fig. 2A (15 min time-lapse/1 min imaging intervals). Anterior is to the top and dorsal to the right.



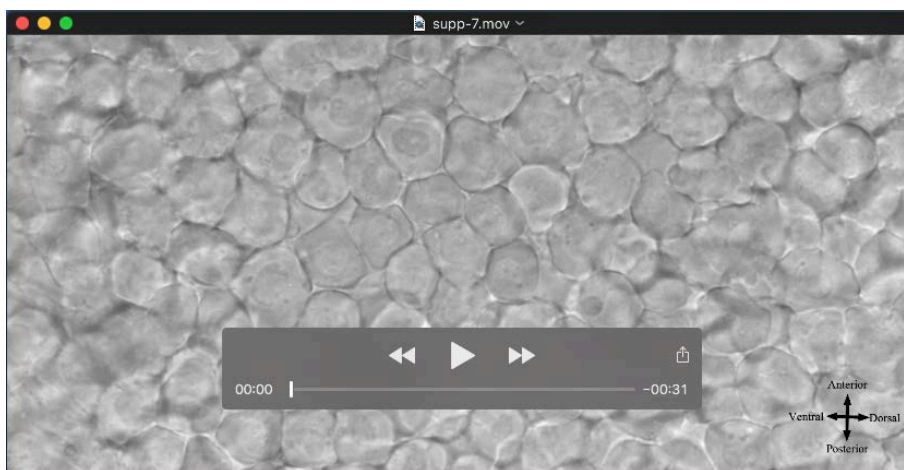
Movie 3. Wild-type embryo + Lifeact-GFP mRNA at *ypc/tb*. Confocal time-lapse imaging of mesodermal cells located 90° from the notochord and near the embryo equator as shown in Fig. 2A (15 min time-lapse/1 min imaging intervals). Anterior is to the top and dorsal to the right.



Movie 4. Wild-type embryo at 80% epiboly. DIC time-lapse imaging of hypoblast/mesendodermal cells located 90° from the notochord and near the embryo equator as shown in Fig. 2A (15 min time-lapse/30 s imaging intervals). Anterior is to the top and dorsal to the right. Select bleb protrusions are highlighted with arrowheads.



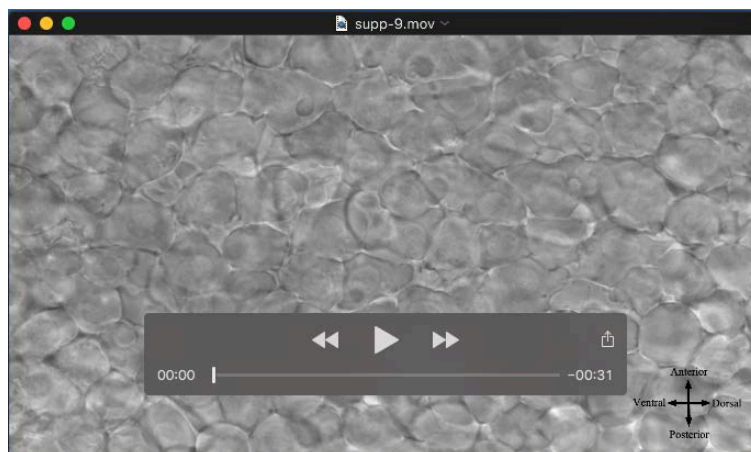
Movie 5. Wild-type embryo at *ypc/tb*. DIC time-lapse imaging of mesodermal cells located $40\text{-}60^\circ$ from the notochord and near the embryo equator as shown in Fig. 2A (15 min time-lapse/30 s imaging intervals). Anterior is to the top and dorsal to the right. Select bleb protrusions are highlighted with arrowheads.



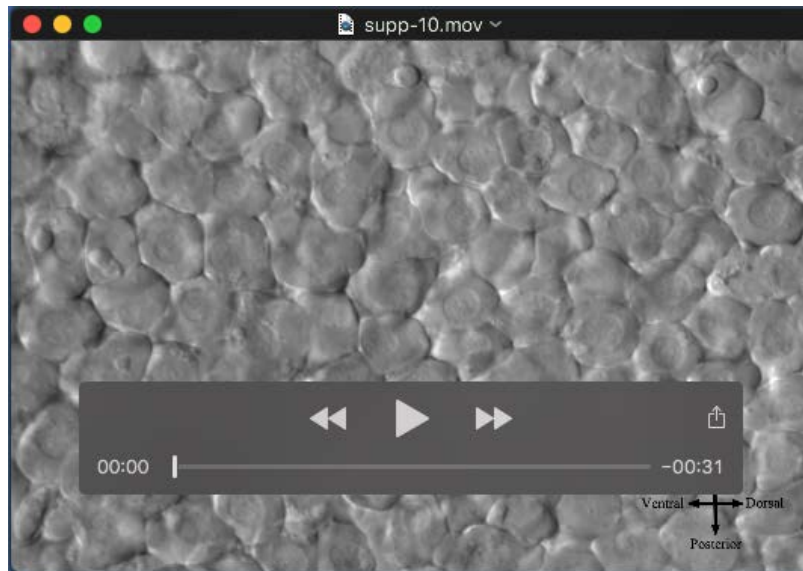
Movie 6. Wild-type embryo + *ca-ezrb* mRNA at 80% epiboly. DIC time-lapse imaging of hypoblast/mesodermal cells located 90° from the notochord and near the embryo equator as shown in Fig. 2A (15 min time-lapse/30 s imaging intervals). Anterior is to the top and dorsal to the right. Select bleb protrusions are highlighted with arrowheads.



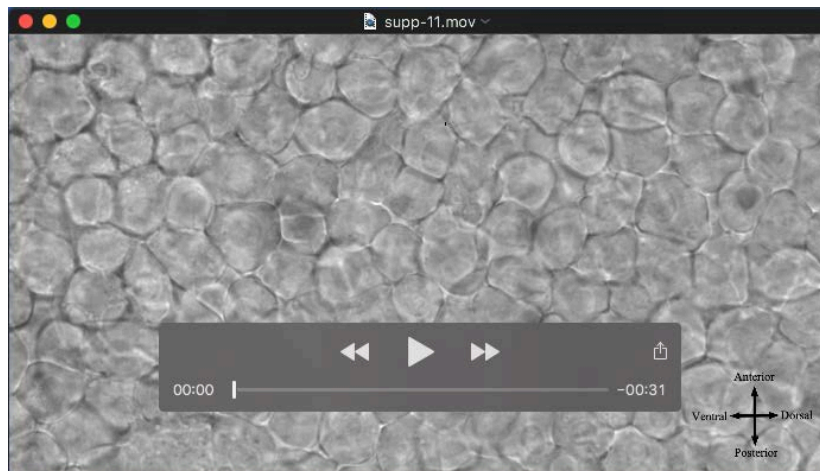
Movie 7. Wild-type embryo + *ezrb* MO at *ypc/tb*. DIC time-lapse imaging of mesodermal cells located 40-60° from the notochord and near the embryo equator as shown in Fig. 2A (15 min time-lapse/30 s imaging intervals). Anterior is to the top and dorsal to the right. Select bleb protrusions are highlighted with arrowheads.



Movie 8. Wild-type embryo + *fn1a/1b* MO at *ypc/tb*. DIC time-lapse imaging of mesodermal cells located 40-60° from the notochord and near the embryo equator as shown in Fig. 2A (15 min time-lapse/30 s imaging intervals). Anterior is to the top and dorsal to the right. Select bleb protrusions are highlighted with arrowheads.



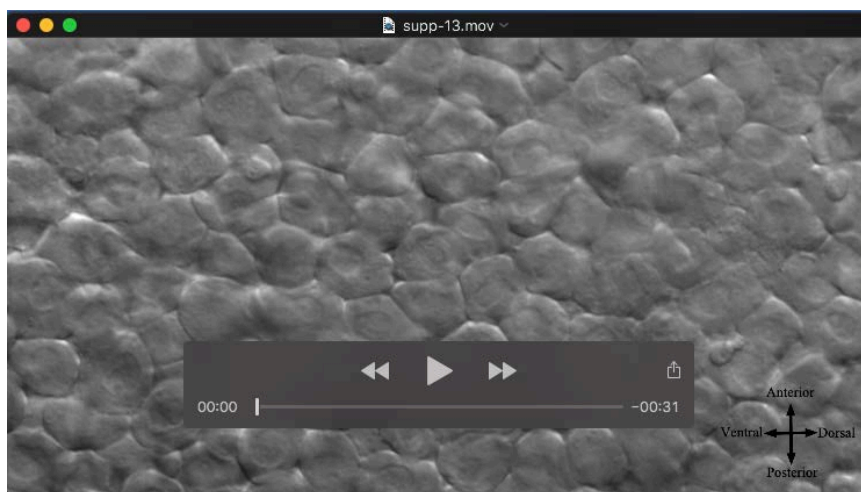
Movie 9. Wild-type embryo + *cdh2* MO at *ypc/tb*. DIC time-lapse imaging of mesodermal cells located 40-60° from the notochord and near the embryo equator as shown in Fig. 2A (15 min time-lapse/30 s imaging intervals). Anterior is to the top and dorsal to the right. Select bleb protrusions are highlighted with arrowheads.



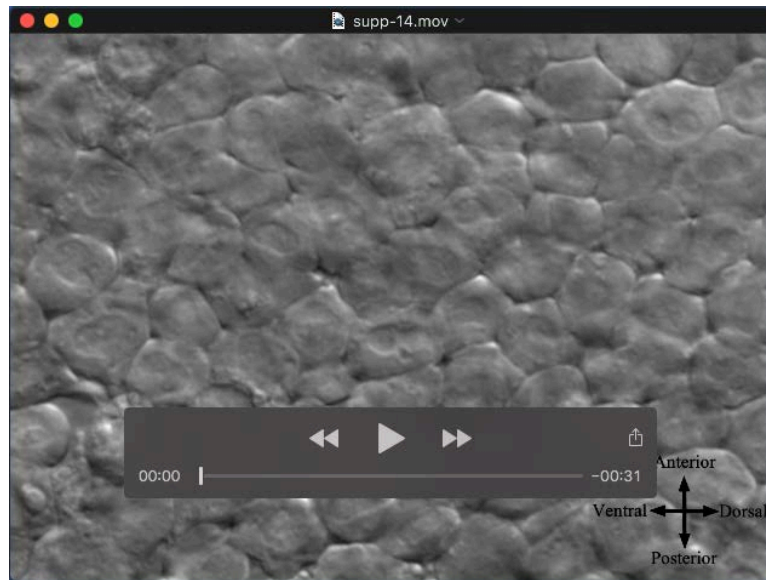
Movie 10. Wild-type embryo + *fn1a/1b* mRNA at 80% epiboly. DIC time-lapse imaging of hypoblast/mesendodermal cells located 90° from the notochord and near the embryo equator as shown in Fig. 2A (15 min time-lapse/30 s imaging intervals). Anterior is to the top and dorsal to the right. Select bleb protrusions are highlighted with arrowheads.



Movie 11. *vangl2*^{vu67/vu67} mutant embryo at *ypc/tb*. DIC time-lapse imaging of mesodermal cells located 40-60° from the notochord and near the embryo equator as shown in Fig. 2A (15 min time-lapse/30 s imaging intervals). Anterior is to the top and dorsal to the right. Select bleb protrusions are highlighted with arrowheads.



Movie 12. *vangl2*^{vu67/vu67} mutant embryo + *ca-ezrb* mRNA at *ypc/tb*. DIC time-lapse imaging of mesodermal cells located 40-60° from the notochord and near the embryo equator as shown in Fig. 2A (15 min time-lapse/30 s imaging intervals). Anterior is to the top and dorsal to the right. Select bleb protrusions are highlighted with arrowheads.



Movie 13. *vangl2^{vu67/vu67}* mutant embryo + *fn1a/1b* mRNA at *ypc/tb*. DIC time-lapse imaging of mesodermal cells located 40-60° from the notochord and near the embryo equator as shown in Fig. 2A (15 min time-lapse/30 s imaging intervals). Anterior is to the top and dorsal to the right. Select bleb protrusions are highlighted with arrowheads.

Fig. S1. Schematic diagrams of methods used to quantify protrusion polarity and PCP.

(A) Filopodia and large lamellipodia-like protrusion polarity were determined in relation to dorsal-ventral body axis. Protrusions were arbitrarily considered aligned if they were oriented $\pm 45^\circ$ relative to the dorsal-ventral axis. (B) Since bleb protrusions were examined at 80% epiboly, the stage when wild-type mesendodermal cells meander toward the dorsal body axis, polarity was determined in relation to the individual cell migration path. Paths were determined by following the frames from time-lapse movies. Lines were drawn through the cell center along the path of movement and through the center of the bleb protrusion and the angles were obtained. Bleb protrusions were arbitrarily considered aligned if they were oriented $\pm 45^\circ$ relative to the path of migration. (C) The length-width ratio of gastrula cells was determined by dividing cell length by cell width as measured at the greatest distances. A value of ~ 1.6 is found in wild-type lateral mesodermal cells at late gastrulation; a value of ~ 1.3 is typical for *vangl2* mutants. (D) Mediolateral alignment is calculated by measuring the angle between lines drawn along the dorsal-ventral body axis and the long axis of the cell. Cells were considered aligned if their long axis is oriented $\pm 20^\circ$ relative to the dorsal-ventral axis.

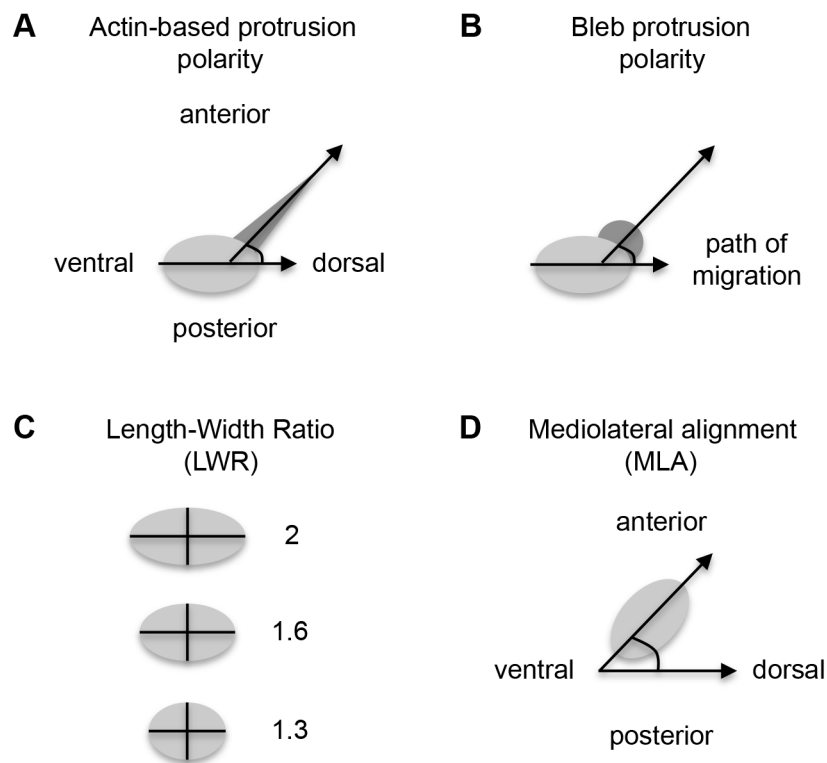


Fig. S2. *ezrb* morpholino injected embryos have mediolaterally broadened mesoderm. Live embryo and whole-mount in situ hybridization (WISH) images of ypc/tb stage embryos. Dorsal views with anterior to the top. Black lines denote notochord (arrow) widths near the embryonic equator of live embryos. White lines highlight the width of paraxial/lateral mesoderm as shown by *protocadherin 8* (*pcdh8*) staining. n, notochord. The *ezrb* morphant paraxial/lateral mesoderm is approximately 10% wider than controls.

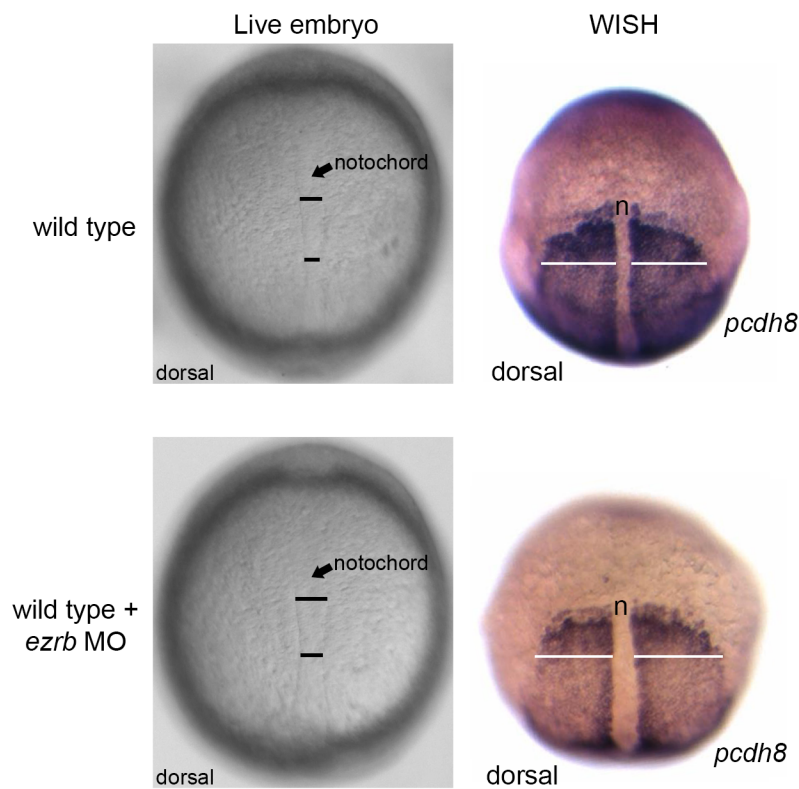


Fig. S3. DIC time-lapse image series showing bleb formation at the *ypc/tb* stage. Depicted are representative images from our time-lapse analyses of wild type control and morphant embryos. Images shown are separated by 30 s time intervals and white arrows denote forming and retracting bleb protrusions. Images are oriented with anterior to the top and dorsal to the right. Scale bars, 5 μ m.

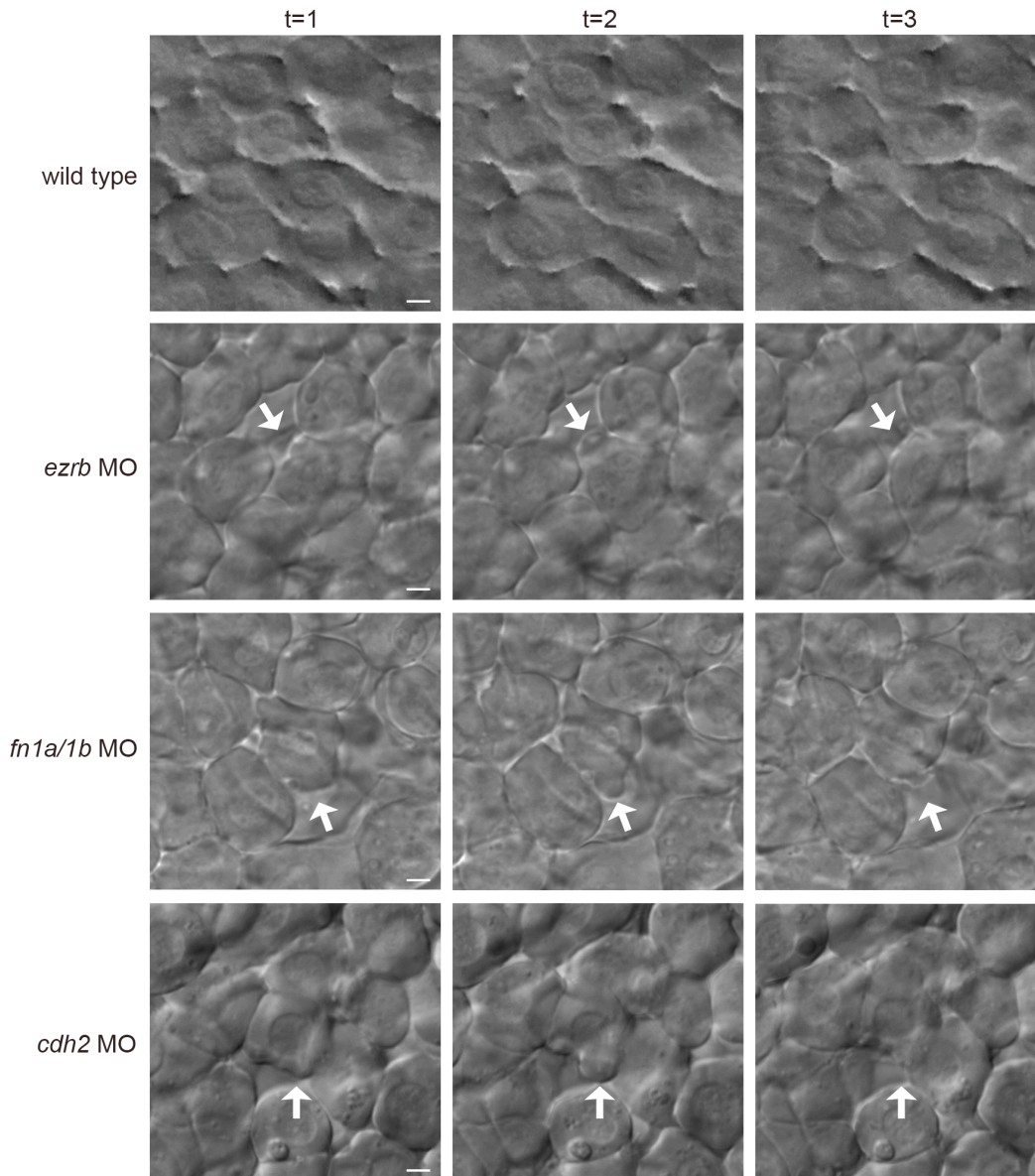


Fig. S4. DIC time-lapse image series showing bleb formation at the 80% epiboly stage. Depicted are representative images from our time-lapse analyses of wild type control and mRNA injected embryos. Images shown are separated by 30 s time intervals and white arrows denote forming and retracting bleb protrusions. Images are oriented with anterior to the top and dorsal to the right. Scale bars, 5 μ m.

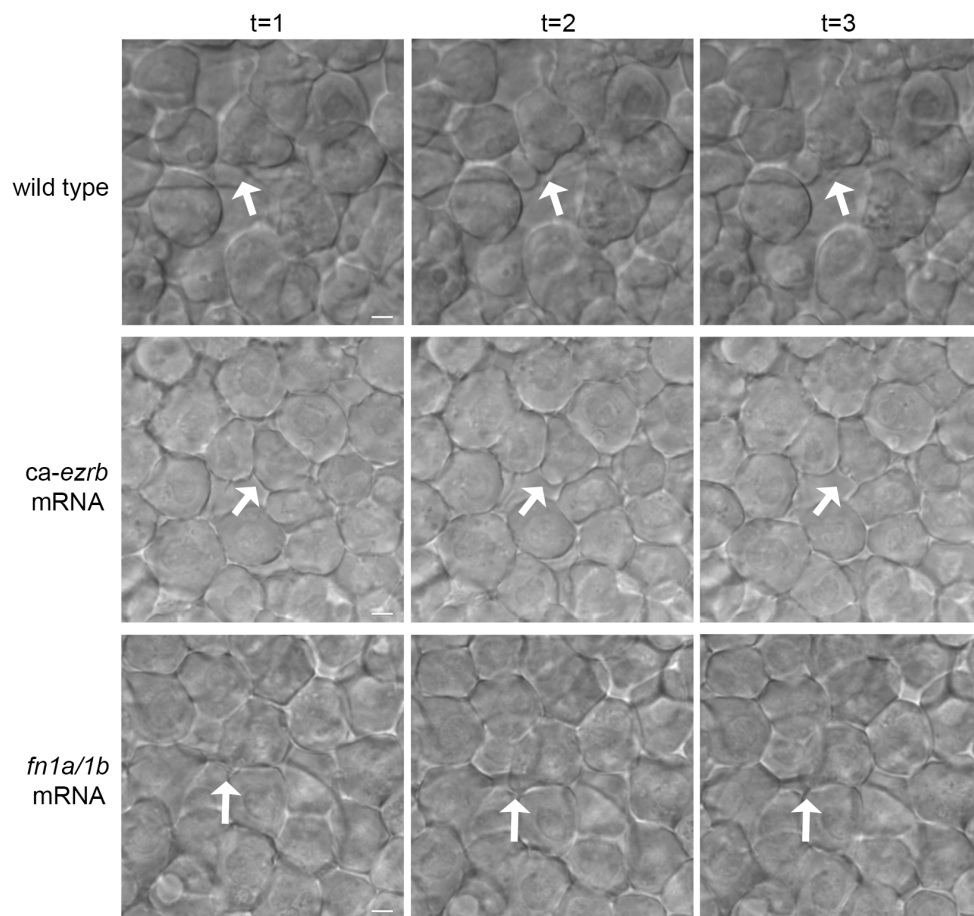


Fig. S5. DIC time-lapse image series showing bleb formation at the *ypc/tb* stage. Depicted are representative images from our time-lapse analyses of *vangl2* mutant control and mRNA injected embryos. Images shown are separated by 30 s time intervals and white arrows/arrowheads denote forming and retracting bleb protrusions. Images are oriented with anterior to the top and dorsal to the right. Scale bars, 5 μ m.

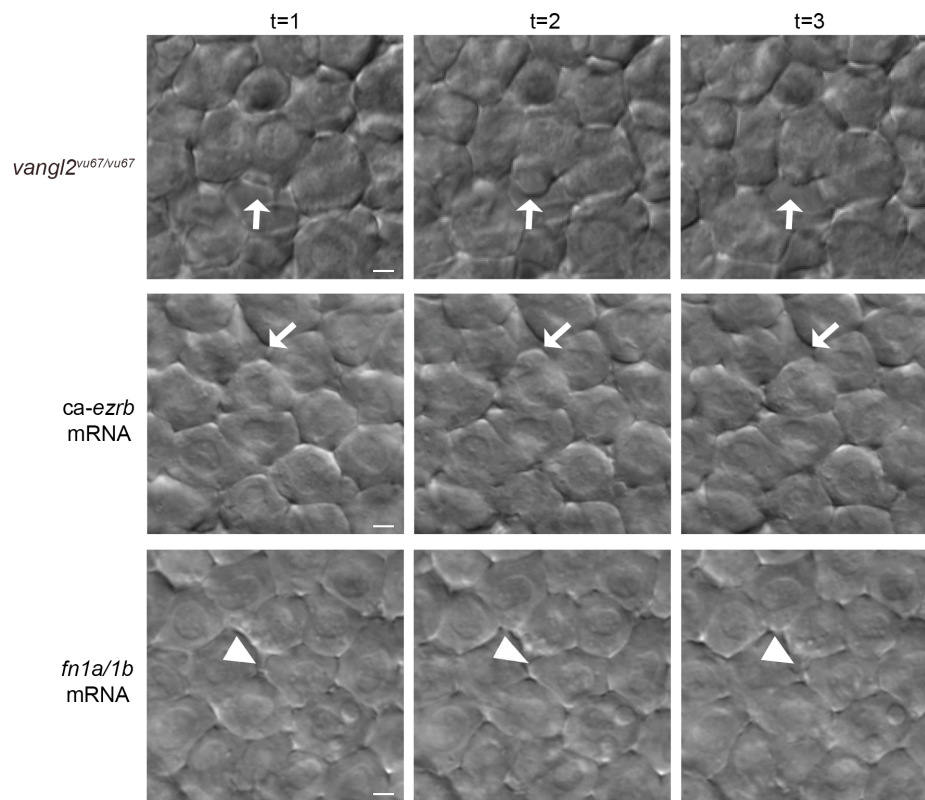


Fig. S6. Bleb protrusions per cell. Quantitation of the number of blebs formed per cell for wild type, mRNA/MO injected, and mutant embryos. Box plots show the interquartile dataset, the median, and the data range. * $P < 0.05$, ** $P < 0.01$; unpaired Student's t-test with Welch's correction.

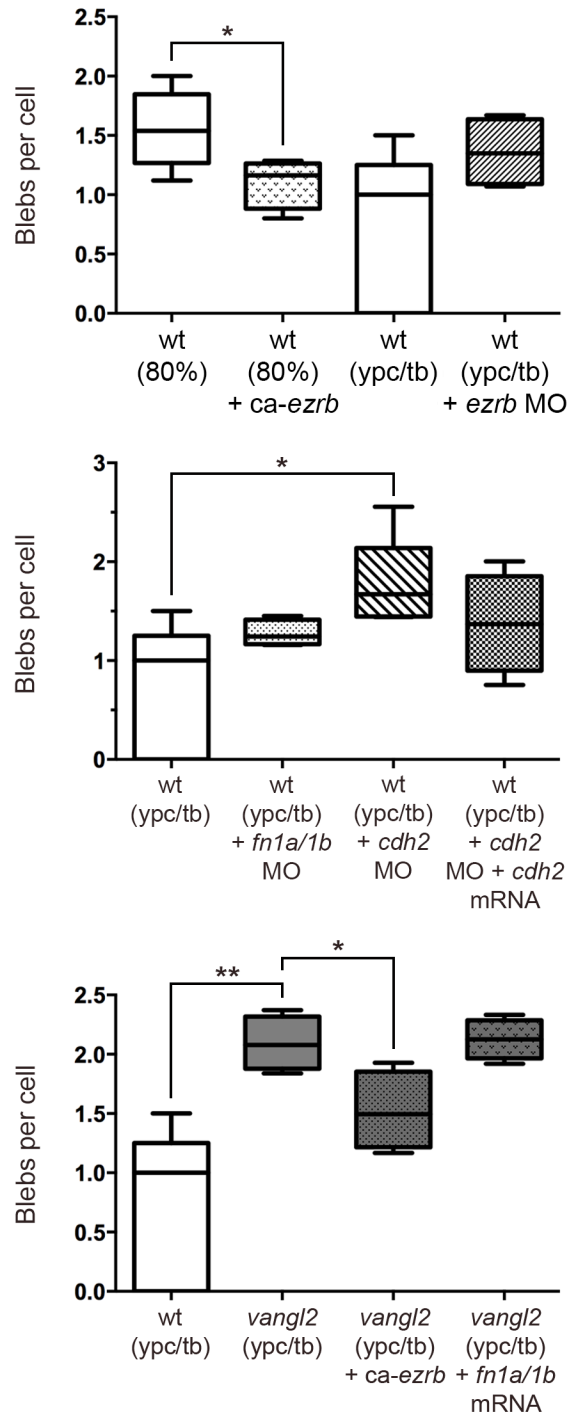


Fig. S7. Rose diagrams depicting MLA of gastrula cells. Bidirectional Rose diagrams correspond to the MLA angular data shown in Figs 4D, 5E, and 7B. The size of the gray shading indicates cell number at specific angles. Mesendodermal (80% epiboly) and mesodermal (yolk plug-closure/tailbud) cell data are shown.

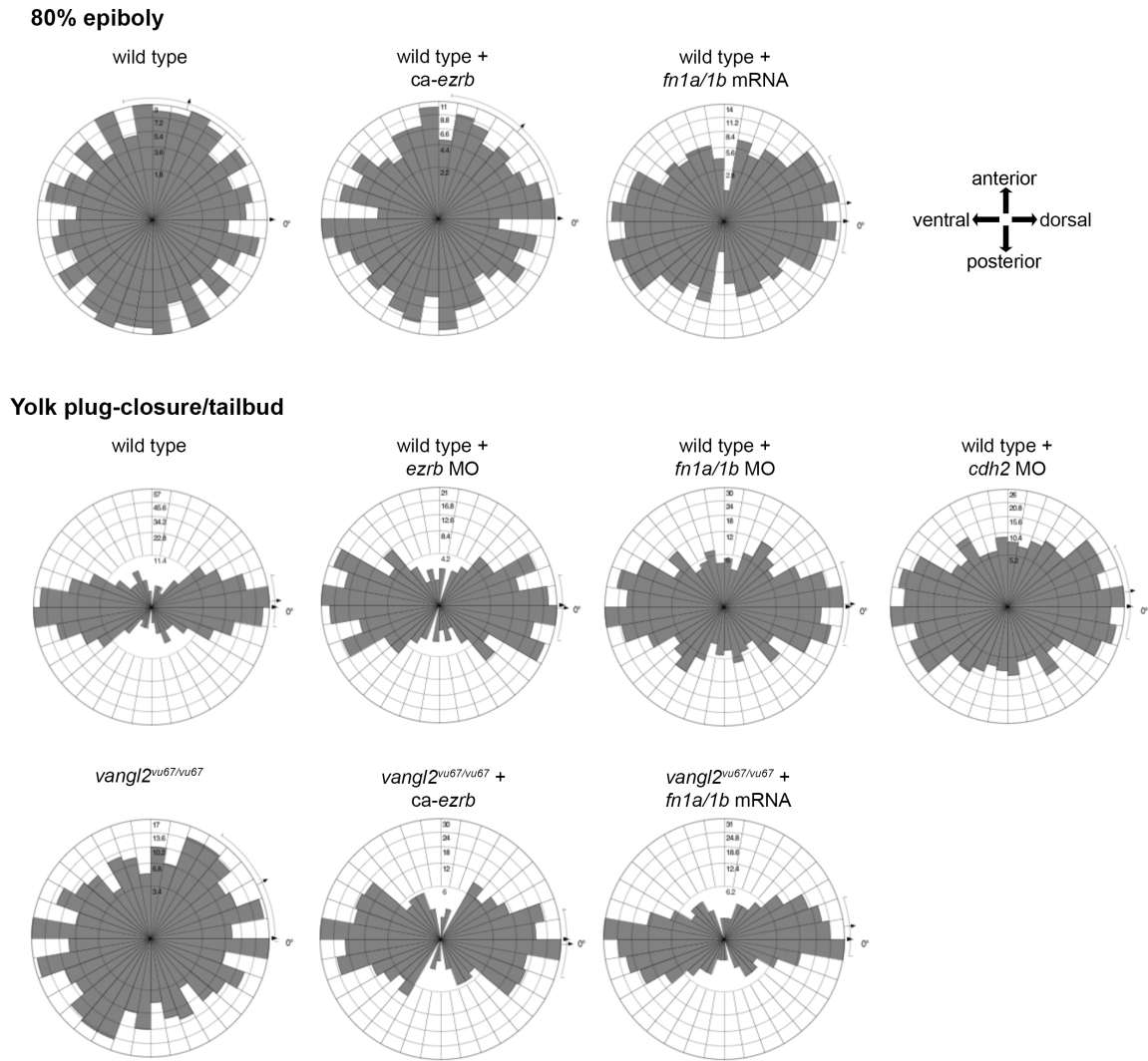


Fig. S8. *cdh2^{tm101/tm101}* mutant embryos recapitulate *cdh2* morphant phenotypes.

Twelve embryos from a *cdh2^{tm101/+}* incross were randomly selected and subjected to DIC time-lapse imaging (5 min with 30 s sampling intervals). Each embryo was genotyped using PCR amplification of genomic DNA and sequencing. Homozygous *cdh2^{tm101/tm101}* embryos have a T->A base-change at amino acid Tyr 514 that introduces a stop codon (Lele et al., 2002). (A) Genotyping results. (B) Representative images from our time-lapse analyses. Images shown are separated by 30 s time intervals and white arrows denote forming and retracting bleb protrusions. Images are oriented with anterior to the top and dorsal to the right. Scale bars, 5 μ m. (C) Germline *cdh2* mutant embryos have defective PCP and greater mesodermal blebbing (*cdh2^{+/+}* siblings and *cdh2^{tm101/tm101}* mutants, n=50 cells for PCP analysis, n=280 cells for bleb analysis, 2 embryos per genotype). * P <0.05, *** P <0.001, **** P <0.0001; unpaired Student's t-test with Welch's correction.

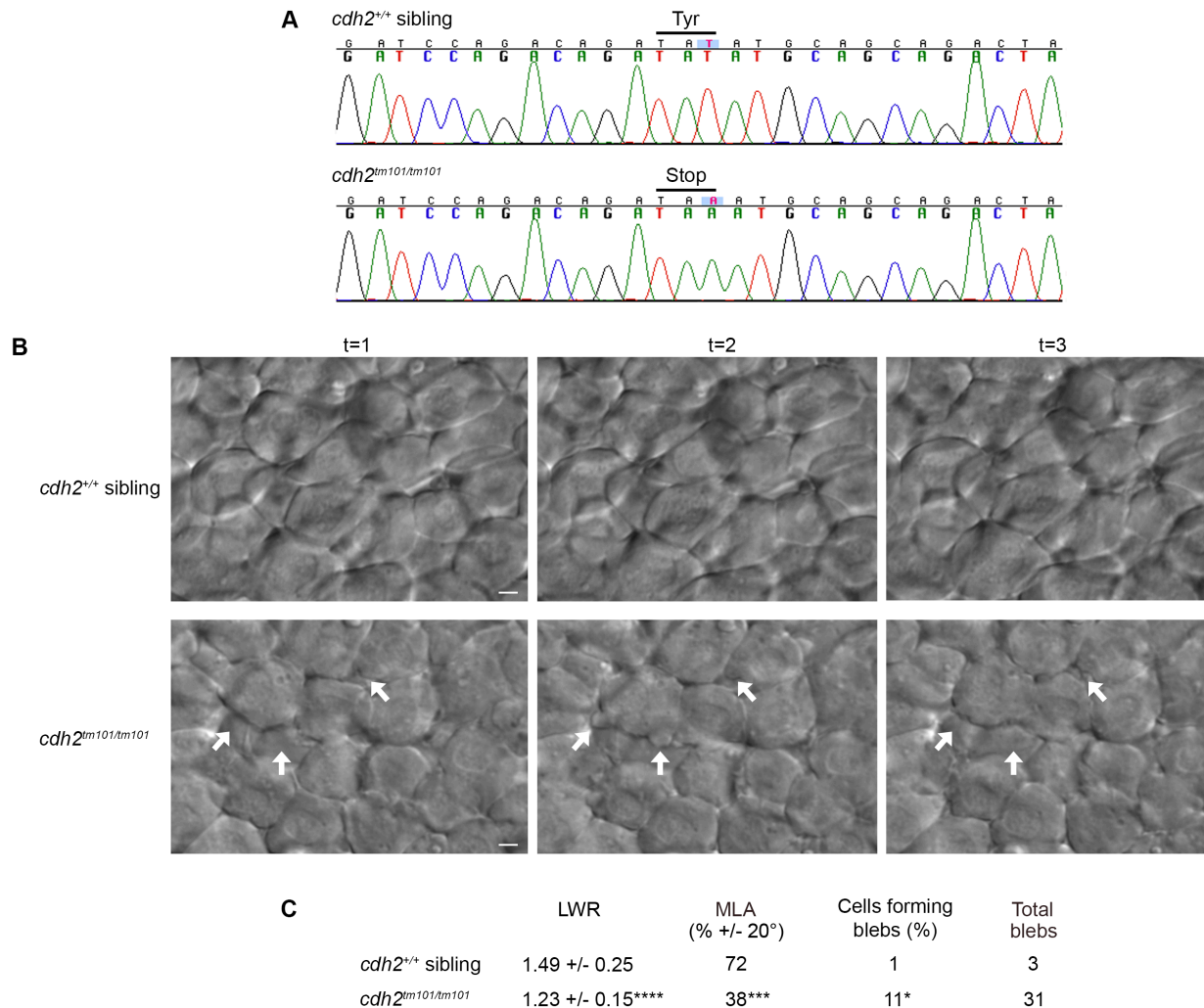


Fig. S9. Western blot analysis showing Ezrb and Cdh2 knockdown. Representative blots of total protein extracts from *ypc/tb* stage *ezrb* and *cdh2* MO injected wild-type embryos (repeated two times). Blots were stripped and re-probed using a β -actin antibody. Relative densitometry values are indicated beneath each lane. The pan-cadherin antibody recognizes an epitope that is conserved between Cdh2 and E-cadherin (Cdh1).

